

## Spin-polarized photoelectron diffraction and valence-band photoemission from MnO(001)

B. Hermsmeier,\* J. Osterwalder,† D. J. Friedman,‡ B. Sinkovic,§ T. Tran, and C. S. Fadley  
*Department of Chemistry, University of Hawaii, Honolulu, Hawaii 96822*

(Received 11 June 1990)

Spin-polarized photoelectron diffraction (SPPD) has previously been proposed as a technique for studying short-range magnetic order in magnetic materials, and the first experimental study of this kind was performed on the ionic antiferromagnetic  $\text{KMnF}_3$  [B. Sinkovic, B. Hermsmeier, and C. S. Fadley, *Phys. Rev. Lett.* **55**, 1227 (1985)]. We present here a much more detailed study of SPPD for the antiferromagnetic transition-metal oxide MnO with a (001) surface orientation. The Mn 3s and Mn 3p multiplets have been studied using both low-energy (192.6 eV) and high-energy (1486.7 eV) x-ray excitation and the intensity ratios  $I(^5S(\uparrow))/I(^7S(\downarrow))$  and  $I(^5P(\uparrow))/I(^7P(\downarrow))$  have been measured as a function of both direction and temperature. Data obtained with the lower excitation energy and resulting in kinetic energies of 50–100 eV show an abrupt change or step in both the  $I(^5S(\uparrow))/I(^7S(\downarrow))$  and  $I(^5P(\uparrow))/I(^7P(\downarrow))$  intensity ratios at  $\approx 530 \pm 20$  K or  $\approx 4.5$  times the Néel temperature  $T_N$ . This change is interpreted to be a new type of short-range-order transition occurring at what is denoted  $T_{SR}$ . Also, these same quintet or septet intensity ratios show a weak peak at  $T_N$ , suggesting for the first time that SPPD has sensitivity to long-range magnetic order. Data obtained for the  $I(^5S(\uparrow))/I(^7S(\downarrow))$  intensity ratio with the higher excitation energy show no such effects, a result consistent with the much weaker exchange scattering expected at such energies. Additional x-ray photoelectron spectroscopy spectra and azimuthal scans of Mn and O core-level intensities are considered and these establish that (i) the sample surface had good stoichiometry and was very clean and well ordered, (ii) the SPPD effects observed at  $T_{SR}$  are not due to any surface structural change, and (iii) a single-scattering cluster (SSC) theoretical model is at least a qualitatively reasonable starting point for describing such effects. We also compare experimental results for the magnitudes of these steps with calculations based upon exchange scattering in the spin-polarized SSC model [B. Sinkovic and C. S. Fadley, *Phys. Rev. B* **31**, 4665 (1985)], and conclude that there is at least qualitative agreement. A final aspect of our data concerns the temperature dependence of the Mn 3d-dominated valence-band spectra: These spectra are found to show no measurable change in crossing  $T_{SR}$ , but by contrast exhibit a large 0.4-eV increase in width in going below  $T_N$ , which is in contradiction to recent theoretical predictions.

### I. INTRODUCTION

The use of spin-polarized photoelectron diffraction (SPPD) as a new technique for studying surface and near-surface short-range spin order in magnetic materials has previously been discussed from both theoretical<sup>1,2</sup> and experimental<sup>3–5</sup> points of view. A principal positive feature of this technique in comparison to other surface-sensitive probes of magnetic order,<sup>6–8</sup> such as the spin-polarized versions of low-energy electron diffraction, Auger spectroscopy, photoemission, inverse photoemission, or electron microscopy, is that in SPPD the origin of the spin-resolved electrons is *internal* to the sample, and thus the electron spins are referenced directly to the local magnetic lattice around a given emitter. This yields two important consequences: First, SPPD studies do not require an *external* spin detector or an *external* spin-polarized source, thereby greatly reducing the difficulty of the experiment. Second, because of this internal referencing, SPPD is capable of investigating magnetic systems more complex than simple ferromagnets; that is, there is no requirement that the sample have a macroscopic magnetic moment (net magnetization). Thus, SPPD is particularly well suited for studying systems

with antiferromagnetic order, and the first observations of such effects were in fact for the antiferromagnet  $\text{KMnF}_3$ .<sup>3</sup> The time scale of photoemission is also very short (approximately  $10^{-16}$ – $10^{-17}$  sec), thus making it considerably faster than that of some other techniques currently used for studying short-range magnetic order such as neutron scattering,<sup>9</sup> but comparable in time scale to that of the very surface-sensitive two-electron capture by deuterons.<sup>10</sup>

The spin-polarized electrons in SPPD arise from an exchange-split outer core-level multiplet in a high-spin ion. For all studies to date, the  $\text{Mn}^{2+}$  ion in a high-spin state of  $[3s^2 3p^6 3d^5]^6S$  has been used. Emission of a 3s electron from this ion produces an easily resolved doublet with a separation of about 6 eV. Such multiplet splittings in ionic solids have been known for some time<sup>11–15</sup> and arise primarily via intra-atomic final-state *L-S* term splittings. In *s* emission this gives rise to a peak separation proportional to  $[2S + 1]K(3s-3d)$ , where *S* is the initial-state spin and *K* is the 3s-3d exchange integral, a result that is derived from the Van Vleck theorem.<sup>11,14,15</sup> For high-spin  $\text{Mn}^{2+}$ ,  $S = \frac{5}{2}$  and the final ionic states with a 3s hole are  $[3s^1 3p^6 3d^5]$  coupled to  $^5S$  and  $^7S$ ; the predicted splitting in simple one-electron Hartree-Fock theory is

approximately 13 eV. Bagus, Freeman, and Sasaki<sup>12</sup> went beyond this simple interpretation by pointing out that more correct final-state wave functions for the  $^5S$  and  $^7S$  states could be obtained from a final-state configuration-interaction (CI) approach. The inclusion of CI was found to yield  $^5S$ - $^7S$  separations of about 6 eV that are in much better agreement with experiment. Within either model of these splittings, the two dominant photoelectron peaks in the  $3s$  multiplet can be considered to be highly spin polarized. If the emitter is taken to be spin up, the predicted polarizations in these peaks are 71% spin down in the  $^7S$  peak and 100% spin up in the  $^5S$  peak.<sup>1(b),2(b)</sup> More recent data by Hermsmeier *et al.*<sup>16(a)</sup> have served to confirm this essentially intra-atomic interpretation of such spectra in solids. In this work, outer core-level  $3s$  and  $3p$  spectra from gas-phase atomic Mn have been compared with those from the solids  $MnF_2$ ,  $MnO$ , and  $Cd_{0.3}Mn_{0.7}Te$  and it was found that the multiplet structures (including weaker CI satellites not discussed here) are essentially identical. This study thus strongly supports the idea of spin-resolved  $3s$  and  $3p$  spectra in these multiplets. This intra-atomic, unscreened interpretation of these multiplets has more recently been confirmed in a theoretical analysis by Kinsinger *et al.*;<sup>16(b)</sup> they conclude that final-state screening effects are only important for  $3d$  compounds containing  $Ni^{2+}$  and  $Cu^{2+}$ . Even in the presence of screening, the observed multiplets may be spin polarized, but their interpretation becomes more complex.

Given such an internally referenced source of spin-polarized electrons, the origin of SPPD effects then lies in differences in the scattering of spin-up and spin-down photoelectrons from the magnetic moments of neighboring atoms as these electrons leave a single-crystal specimen. Prior discussions of SPPD have focused on the exchange term in the *elastic* scattering potential as the origin of this asymmetry,<sup>2,3</sup> and we shall adopt this point of view also in the discussion here. It is also possible that inequivalent *inelastic* scattering for spin-up and spin-down electrons may play a role, although this is expected to be a smaller effect.<sup>2(b),6,7,17</sup> as discussed further below. Additional effects due to spin-orbit scattering might also have to be included in a fully accurate treatment of these effects,<sup>6</sup> but these have so far been neglected in considering antiferromagnetic systems, primarily because of the canceling nature of the antiparallel spins. In photoelectron diffraction (PD) without spin resolution, SPPD effects will usually be averaged out because the neighboring ions either have zero magnetic moments or moments that are randomly oriented relative to a given emitter.

Photoelectron diffraction at energies above a few hundred eV has been found to be well modeled by single-scattering cluster (SSC) calculations with the inclusion of spherical-wave (SW) scattering.<sup>18</sup> PD effects at energies as low as 100 eV have been semiquantitatively predicted in this way.<sup>18(b),18(c),18(e)</sup> Within this model, photoelectron emission gives rise to an outgoing spherical wave which is attenuated due to both the usual  $1/r$  factor and exponential inelastic effects. This strong attenuation makes photoelectron diffraction in general a short-range near-neighbor probe much like surface extended x-ray-

absorption fine structure (SEXAFS).<sup>18</sup> The extension of the SSC model to a spin-polarized case involves the correct inclusion of the  $3d$  exchange term in the atomic potentials that are used to create the muffin-tin potential from which scattering phase shifts are derived, as discussed in detail elsewhere.<sup>2</sup> However, a fully accurate treatment of the exchange interaction for free electrons is not available.<sup>6,19</sup> Thus, in the calculations presented here, we have used two different density-functional exchange approximations to calculate spin-dependent phase shifts:<sup>2</sup> the Dirac-Hara<sup>20</sup> (DH) approximation with an energy-dependent  $\alpha$  parameter and the Kohn-Sham<sup>21</sup> (KS) approximation with an  $\alpha$  constant of  $\frac{2}{3}$ . Since KS is expected to be too strong for free electrons and it has also recently been realized that DH may fall off too fast with increasing energy,<sup>19</sup> our results are expected to approximately bracket the correct values.

The first SPPD studies by Sinkovic *et al.*<sup>2,3</sup> dealt with the antiferromagnet  $KMnF_3$ . For this system, it was found that an abrupt change in the spin-up to spin-down or  $I(^5S)/I(^7S)$  intensity ratio occurred well above the Néel temperature at approximately  $2.7T_N$  or 240 K. No change in this ratio was noted on going toward  $T_N$ . This abrupt change well above  $T_N$  was suggested to be due to a sudden decrease of the short-range antiferromagnetic order around a given emitter at a temperature that was termed the short-range order transition temperature  $T_{SR}$ . Diffraction calculations as discussed above yield results that agree qualitatively with the signs and magnitudes of the effects seen in experiment.<sup>2</sup> More recent heat-capacity data that have been obtained on  $KMnF_3$  (Ref. 22) further show a small peak near  $T_{SR}$  that may be connected with this loss of short-range order. However, there are at present no theoretical calculations based upon the statistical mechanics of such spin systems that predict such a sharp loss of short-range order at a temperature well above the Néel temperature.<sup>2(b),23-26</sup> In another recent SPPD study, Johnson, Starnberg, and Hughes<sup>5</sup> reported spin-up to spin-down intensity ratio changes in the  $Cr^{3+}$   $3s$  multiplet found in  $NaCrS_2$ . These measurements were made at high and low temperatures, but did not involve a detailed study of temperature dependence; thus, no conclusions regarding the presence or absence of a sharp short-range-order transition can be drawn from this work.

It is therefore of considerable interest to see whether such effects are found in other materials and to begin to establish their systematics. To this end, we have made a detailed study of such effects in antiferromagnetic MnO. A preliminary account of this work appears elsewhere,<sup>27</sup> but we present here considerably more experimental data and also compare theoretical and experimental SPPD effects for this system.

MnO is of interest for such a study for several reasons. Its high-spin  $Mn^{2+}$  ions exhibit a well-resolved  $3s$  doublet with a 6.0-eV spacing that is well suited for monitoring SPPD effects. The possible existence of short-range magnetic order at temperatures up to approximately 200° above the Néel temperature of  $T_N = 120$  K has been postulated for MnO based upon neutron-diffraction studies

of its antiferromagnetic structure.<sup>9</sup> However, to our knowledge, no systematic studies have been carried out to monitor this proposed short-range order as a function of temperature.

MnO (manganosite) is a type-II antiferromagnet with a Néel temperature ( $T_N$ ) of 118–120 K.<sup>28</sup> It has the sodium chloride structure with a lattice constant of 4.445 Å at ambient conditions that decreases smoothly to 4.437 Å at  $T_N$ , where the crystal undergoes a small cubic-to-rhombohedral lattice distortion of  $\approx 0.5^\circ$  due to a contraction along the [111] antiferromagnetic direction. The lattice constant then again smoothly decreases to  $\approx 4.431$  Å at liquid-helium temperatures.<sup>28,29</sup> Apart from this cubic-to-rhombohedral transition, there are no other structural phase transitions known over the full range of temperatures used in this study (60–900-K range), with all changes in the lattice constant being smooth functions of temperature except at the Néel temperature.<sup>28</sup> Heat-capacity data for room temperature and below also show no anomalies except at the Néel temperature.<sup>30</sup>

We report here for MnO the most detailed study to date of SPPD effects and their relationship to short-range magnetic order (SRMO). A single crystal of this antiferromagnet with (001) surface orientation has been studied with both low-energy (Mo  $M\zeta=192.6$  eV) and high-energy (Al  $K\alpha=1486.7$  eV) excitations and for emission from two different core levels: Mn 3s and Mn 3p. (Prior SPPD work has involved only 3s emission.<sup>2–5</sup>) Data involving both the more common form of photoelectron diffraction without spin resolution and spin-polarized photoelectron diffraction are discussed. In the SPPD portion of the results, the spin-up to spin-down ratio is monitored as a function of both direction and temperature, with fine steps being made in the temperature so as to determine the precise form of what we find to be a short-range-order transition. Other possible causes of the behavior at the short-range-order transition temperature are considered and ruled out. Finally, theory is compared to experiment for both non-spin-resolved and spin-polarized photoelectron diffraction. As an additional aspect of our experimental data, we also present  $3d$  valence-band spectra that show no measurable change in crossing  $T_{SR}$  but a significant change in width on crossing  $T_N$ ; no such effect has been seen before.

## II. EXPERIMENTAL

All photoelectron spectra were obtained with a VG Instruments ESCALAB5 spectrometer equipped with a custom-designed two-axis specimen goniometer<sup>18(a)</sup> and a Surface Science Laboratories Model 3390 multichannel detector<sup>31</sup> for angle-resolved studies. The goniometer permitted high-precision automated rotation of both the polar ( $\theta$ ) and the azimuthal ( $\phi$ ) angles of emission, as defined in Fig. 1. Both angles were controlled to an accuracy of  $\pm 0.3^\circ$ . Temperature variation of the specimen between 60 and 1300 K also was possible. Heating was accomplished with a resistive button heater (Spectra-Mat E-292) situated just below the specimen and inside a molybdenum barrel. Cooling was effected by firmly connecting a Ag-coated Cu braid to the rotating sample

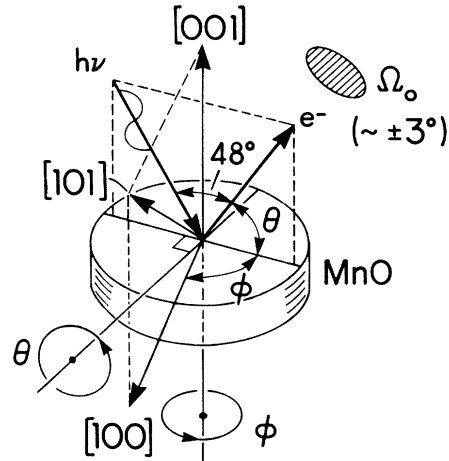


FIG. 1. The experimental geometry, with various angles defined.

holder with a Cu clamp; the other end of the Cu braid was firmly fastened to a specially designed UHV cold finger which could be cooled by either liquid nitrogen or liquid helium. Temperature measurements were made with two Chromel-Alumel thermocouples attached very near the sample, as well as with an infrared pyrometer cross-calibrated against the thermocouples. The estimated absolute accuracy in the temperatures reported here is  $\pm 25^\circ$ , although for a given crystal mounting, the relative temperatures over a scan were known to within  $\pm 10^\circ$  (except over the lowest temperature regions where the reduced response of the thermocouple increased this to  $\pm 20^\circ$ ). Both standard Al  $K\alpha$  (1486.7 eV) radiation and the less commonly used Mo  $M\zeta$  (192.6 eV) radiation were used for excitation. Two Mo anodes constructed as modifications of the standard Cu anode of the spectrometer were used: one consisted simply of a 5-mil-thick Mo foil cap wired to the anode and the other, developed by Scherrer,<sup>32</sup> consisted of 5000 Å of Mo deposited on successive Ni and Cr underlayers to promote adhesion and prevent diffusion. A 50- $\mu\text{g}/\text{cm}^2$  carbon foil window was used to isolate the x-ray source from the sample region. Fully UHV conditions of  $5.0 \times 10^{-11}$  Torr were maintained during all of the measurements reported here.

The specimen used for this study was a single crystal of MnO cut in wafer form with (001) surface orientation; its dimensions were 1.8 mm thick by 9.0 mm diameter. Laue diffraction verified that this orientation was good to within  $\pm 0.4^\circ$ . The most common impurities usually associated with MnO are the higher-order oxides, carbides, and hydroxides such as  $\text{MnO}_2$ ,  $\text{Mn}_2\text{O}_3$ ,  $\text{Mn}_3\text{O}_4$ ,  $\text{MnCO}_3$ , and  $\text{Mn}(\text{OH})_2$ .<sup>28,33–35</sup> Of these,  $\text{MnO}_2$  was suspected of being the most important for our sample because its distinctive brown color was usually present immediately after any cutting or light grinding of the surface. However, polishing was found to remove the brown areas of the surface, leaving the dark green color characteristic of MnO clearly visible.  $\text{MnO}_2$  furthermore decomposes to MnO at approximately 800 K,<sup>28</sup> a temperature normally reached during our *in situ* annealing process. We comment below on the initial presence of some additional im-

purities and the final *in situ* analysis of the specimen surface.

The initial cutting of the sample was done with diamond-cutting tools and an oil-based lubricant to which MnO showed no reactivity. The disc was subsequently polished with 600 grit silicon carbide paper and diamond abrasive pastes of 15-, 8-, 3-, 1-, and 0.25- $\mu\text{m}$  grit size, followed by a final light buff on a lubricated nylon cloth. Crystal alignment was again checked with Laue after the polishing procedure and found to have remained constant. At the end of this process, the surface exhibited a smooth mirror finish, with the only imperfections being some small and highly reflective regions that occupied at most 10% of the surface area. These small blemishes could not be eliminated by repolishing with various recipes and so, to try to assess them further, we examined both the smooth and blemished regions of the surface with scanning electron microscopy (SEM) combined with energy-dispersive x-ray fluorescence spectroscopy (EDXFS). At most, it was found that the blemishes may have approximately 5% less Mn than a smooth surface region, suggesting the possible presence of other manganese compounds. Surface-sensitive grazing-emission x-ray photoelectron diffraction (XPD) measurements, however, showed strong patterns characteristic of a well-ordered NaCl structure, and also gave a stoichiometry very close to that of MnO (see below). Thus, particularly since less than 10% of the surface is affected, these blemishes should have negligible influence on our photoelectron diffraction measurements.

Just after the specimen was placed in the spectrometer, overall x-ray photoelectron spectroscopy (XPS) core spectra revealed several impurities on the surface: C as expected, plus Ca, Si, K, and Al. After repeated cycles of  $\text{Ar}^+$  bombardment at  $\approx 45^\circ$  incidence and  $\approx 500\text{-V}$  energy, followed by annealing at  $\approx 900\text{ K}$ , these impurities could be eliminated from the surface; that is, no impurities were detectable with XPS after this cleaning procedure. However, as discussed in more detail below, Si and Al appeared to be low-level bulk impurities that could segregate to the surface at elevated temperatures, and so care was exercised to avoid their interfering with the Mn spectral regions of interest.

In order to work at lower kinetic energies for which spin-dependent scattering effects are expected to be largest,<sup>2</sup> all of the SPPD studies were done using Mo  $M\zeta$  radiation. In Fig. 2 we compare spectra obtained with Mo  $M\zeta$  and Al  $K\alpha$  excitation for the low-binding-energy region of principal interest in this study. These two spectra contain both of the outer core-level 3s and 3p multiplets that have been used to monitor SPPD effects, as well as the valence-band region. The influence of photoelectric cross-section changes on relative intensities is also apparent, especially for the predominantly 3d valence bands which are much more intense at the lower energies. There is also an increase in the relative intensity of the Al 2p impurity peak at  $\approx 75\text{ eV}$  for low excitation energy, thus making its effects on the region between the  $^7S$  and  $^5P$  multiplet peaks more obvious than in the Al  $K\alpha$  spectrum.

XPS stoichiometries derived from Mn  $2p_{3/2}$  and O 1s

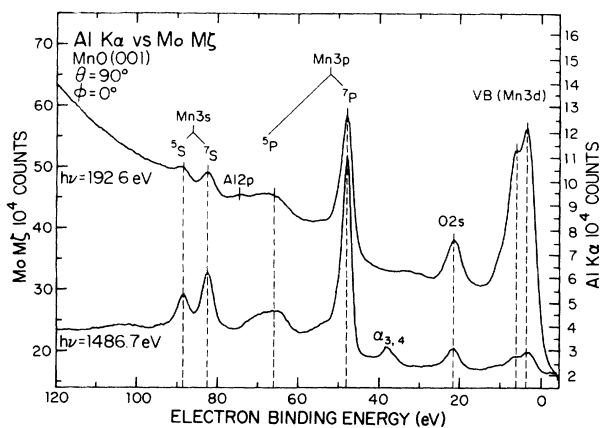


FIG. 2. Comparison of 3s-3p valence overall spectra excited by Mo  $M\zeta$  and Al  $K\alpha$  radiation. Here, the Mn 3s and 3p multiplets are clearly visible, with the peaks of primary interest labeled  $^5S$ ,  $^7S$ ,  $^5P$ ,  $^7P$ . Note also the nature of the backgrounds on which the peaks sit.

intensities and standard analytical formulas<sup>18(a)</sup> were also found to be very close to that of MnO for both normal emission ( $\text{Mn}_{1.0}\text{O}_{1.15}$ ) and more surface-sensitive grazing emission at  $\theta=10^\circ$  ( $\text{Mn}_{1.0}\text{O}_{1.3}$ ). With an estimated accuracy of  $\pm 0.15$  in these numbers, they are thus consistent with having MnO at the surface, although there may be a slight amount of excess oxygen. Under these clean-surface conditions, the sample was found to be extremely stable, with little or no accumulation of impurities onto the surface over a several-day time period involving cycling through the entire temperature range.

As a further analytical probe of the sample chemical state, Fig. 3 shows Al  $K\alpha$ -excited Mn 2p spectra for two emission directions: normal to the surface ( $\theta=90^\circ$ ) with

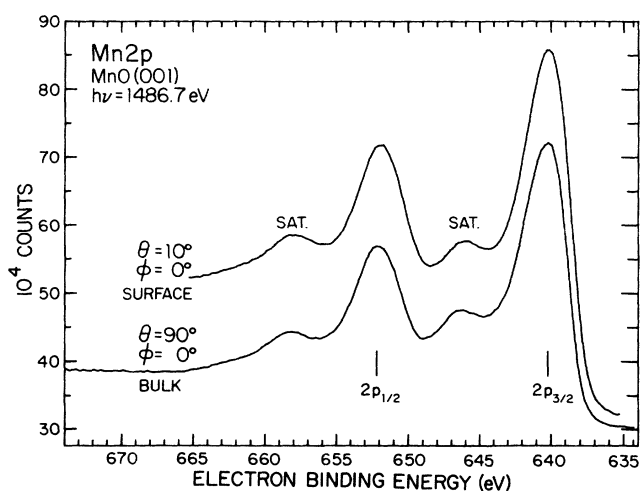


FIG. 3. XPS spectra from the spin-orbit split Mn 2p levels are shown at grazing ( $\theta=10^\circ$ ) and normal ( $\theta=90^\circ$ ) emission. These spectra show the characteristic 2p satellites at  $\approx 6\text{-eV}$  higher binding energy than the main lines; they are evident in both the surface-sensitive  $10^\circ$  spectrum and the more bulk sensitive  $90^\circ$  spectrum.

maximum bulk sensitivity and at a very low angle with respect to the surface ( $\theta=10^\circ$ ) which should have a surface sensitivity comparable to our SPPD measurements with Mo  $M\zeta$  excitation. At both angles, the  $2p$  spectra are very similar, including the positions and relative intensities of the satellites that are well known to be associated with MnO.<sup>33–35</sup> These results thus also indicate an MnO stoichiometry at the surface. This stoichiometry is also confirmed by the identical Mn  $3s$  and  $3p$  multiplet splittings found with more bulk sensitive Al  $K\alpha$  excitation and more surface sensitive Mo  $M\zeta$  excitation (cf. Fig. 2) and the excellent agreement of these splittings with prior studies.<sup>9–14,33</sup>

The need to measure multiplet peak-intensity ratios very precisely for this SPPD study, coupled with the insulating properties of MnO, made it necessary both to maintain impurity levels at constant low values over the entire duration of a temperature scan and to correct for charging effects at lower temperatures.

Of the impurities present on the surface, Si and Al were the most problematic in that they had a tendency to diffuse to the surface at high temperatures and the Si  $2p$  and the Al  $2p$  photoelectron peaks interfered with those of the Mn  $3s$  and  $3p$  multiplets. An indication of this can be seen in Fig. 2, where the Al  $2p$  is seen between the Mn  $3s$  and  $3p$  regions for the Mo  $M\zeta$  spectrum. This surface segregation influenced the choice of annealing temperature, which needed to be high enough to allow the crystal to recover from the sputter damage incurred during the cleaning process and low enough to limit the surface segregation. A temperature of approximately 900 K and a duration of approximately 8 h were found to best accommodate both requirements. In order to minimize such segregation effects, all temperature scans shown in this paper were done in a high to low temperature fashion, with a repeat of the highest temperature point being made at the end as a check for reproducibility.

It was also critical to neutralize any specimen charging effects so that peak relative intensities were not spuriously influenced by resulting peak broadening or shifting. At ambient conditions MnO is known to be a good insulator, with the log of its resistivity being approximately linear with temperature.<sup>36</sup> Charging effects originate from the x-ray-induced removal of primary and secondary electrons from the surface and subsurface regions. The net charge at the surface is dependent on several factors such as the near-surface conductivity, the photon flux, the secondary electron flux from the nearby x-ray isolation window, radiative heating from the x-ray tube, and instabilities in the electron flood gun (Hewlett-Packard Model HP-18623) used to compensate these charging effects. At typical experimental conditions for the operation of the Mo anode with 4 kV and 10 mA or a power of 40 W, charging shifts of about 10 eV were observed at room temperature. The change in conductivity under these conditions was determined by monitoring the Mn  $3p$  peak position with the flood gun off, as is shown in Fig. 4. These results indicate that the near-surface conductivity of MnO steadily increases up to approximately 480 K, at which point the specimen becomes sufficiently conducting as judged by photoemission that no further

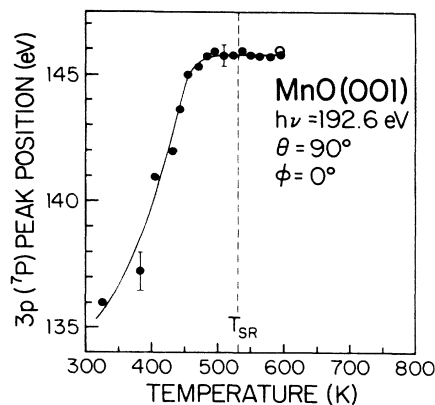


FIG. 4. The temperature dependence of sample charging in MnO under standard experimental operating conditions and with the electron flood gun off. Temperature has been scanned in a downward direction (solid points), with a repeat point for the maximum temperature at the end of the run (open point). Above  $\approx 480$  K the sample region seen in photoemission abruptly comes to behave as a conductor. Note that  $T_{SR}$  is well above this changeover.

peak shifts or broadenings are noted. Furthermore, peak positions are found to remain constant with changes in flood-gun current above 480 K. An interesting observation from this data is thus that the near-surface region of the specimen measured by XPS changes over a rather narrow temperature interval to a state that is sufficiently conducting to eliminate sample charging effects.

For temperatures below 480 K, it was thus necessary to employ the flood gun to neutralize the surface; typical operating parameters were an emission current of  $100 \mu\text{A}$  with a stability of  $\pm 0.5 \mu\text{A}$  and a kinetic energy of 1.0 eV. For maximum consistency, the flood gun was used throughout all critical temperature scans discussed in this paper. At each temperature point, the flood gun was adjusted to yield spectra with the same peak position and resolution as reference spectra taken well above 480 K. However, we note that the short-range magnetic order transition region near  $T_{SR} = 530$  K that will be of principal interest here is well above the point at which the surface becomes conducting, and therefore the precise nature of the charge compensation does not in any way affect our conclusions concerning this transition.

### III. RESULTS AND DISCUSSION

#### A. Verification of near-surface structure by photoelectron diffraction

We begin by considering the degree of crystalline order at the surface of our specimen, since the photoelectron diffraction process has already been shown to be highly sensitive to the degree of near-surface order.<sup>18(b),37,38</sup> Because of the insulating character of MnO at ambient temperature, low-energy electron-diffraction measurements were not possible. Thus, in order to monitor the structure and order in the near-surface region, azimuthal scans of O  $1s$  and Mn  $2p$  intensities were taken at various

polar angles. These were subsequently compared to previously obtained O 1s azimuthal data for NiO(001), which grows in the same NaCl structure on Ni(001),<sup>37</sup> as well as to theoretical simulations with the single-scattering cluster model for ideal MnO(001). These results are shown in Figs. 5–7. The general forms of the experimental azimuthal scans were present from the very first measurements on the sample, but the degree of anisotropy increased with cleaning and annealing in vacuum. That is, if we define the degree of anisotropy in a given scan to be  $(I_{\max} - I_{\min})/I_{\max} = \Delta I/I_{\max}$ , it was found to show a substantial increase from  $\approx 20\%$  initially to  $\approx 50\%$  after the crystal surface was fully prepared for SPPD studies. Prior work shows anisotropies of the order of 50% to be indicative of a very highly ordered surface.<sup>18(b),37,39</sup>

We consider first Fig. 5, which compares an O 1s azimuthal scan from MnO(001) taken with Al  $K\alpha$  radiation at  $\theta=45^\circ$  with an analogous scan from a NiO(001) film grown by oxidation and annealing on Ni(001).<sup>37</sup> The very close agreement in form and anisotropy (48% versus 53%, respectively) between the two scans testifies to the high quality of the MnO near-surface region obtained. In Fig. 6, single-scattering cluster (SSC) calculations for MnO with the inclusion of spherical-wave (SW) scattering are compared to the O 1s data of Fig. 5. Curves making use of both the Kohn-Sham<sup>2,21</sup> (KS) and Dirac-Hara<sup>2,20</sup> (DH) approximations for exchange are shown. There is in general very good agreement here, even as to the degree of anisotropy, which is only overestimated in theory by 13–14%, an amount that can easily be due to the presence of a certain number of defects or blemishes

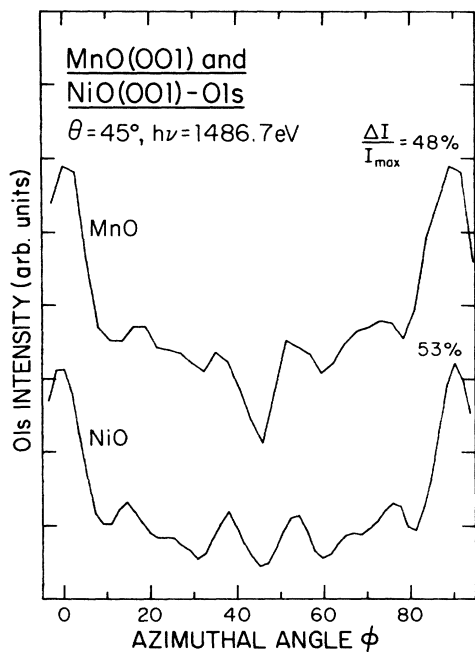


FIG. 5. A comparison of O 1s XPD azimuthal patterns for our MnO(001) crystal and a NiO(001) film grown on a Ni(001) substrate (Ref. 37) indicating a high degree of structural similarity between the two NaCl lattices. The overall anisotropies of  $\Delta I/I_{\max} = (I_{\max} - I_{\min})/I_{\max}$  are given for the two curves.

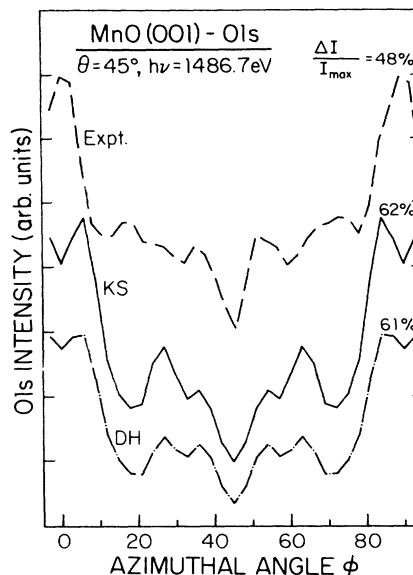


FIG. 6. A comparison of experimental and theoretical O 1s azimuthal scans for MnO(001). The experimental curve is the same as in Fig. 5. The theory displays two SSC-SW curves, one using the Dirac-Hara (DH) energy-dependent exchange interaction in the scattering potential and one using the Kohn-Sham (KS) energy-independent interaction. The nonstructural parameters used were an inner potential of 25 V, an electron mean free path of 8 Å, and Debye-Waller effects appropriate for ambient temperature.

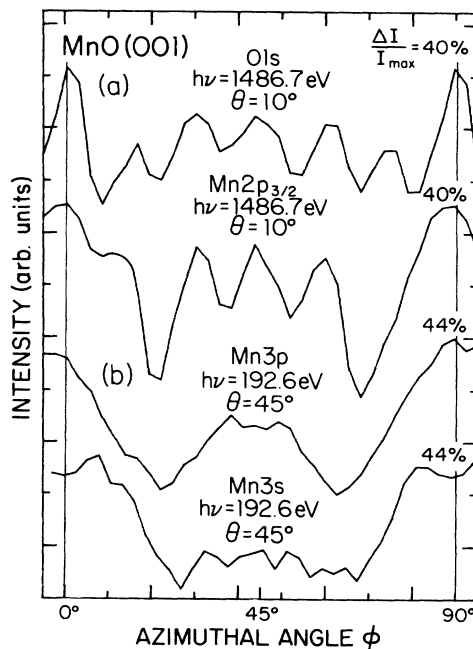


FIG. 7. Four azimuthal scans, all taken under very surface-sensitive conditions of either grazing emission (a) or low energy (b), show the high degree of surface structural order as evidenced by the large anisotropies found. The two curves in (a) were taken at grazing emission ( $\theta=10^\circ$ ) using Al  $K\alpha$  radiation. The spectra in (b) were taken at  $\theta=45^\circ$  using the lower-energy Mo  $M\zeta$  source.

on the surface and/or some degree of multiple scattering. These results thus further indicate the high degree of order obtained on this MnO surface. They also provide further support for the validity of the SSC-SW model for describing such XPD data, including its spin-dependent generalization that will be considered later in this paper. The azimuthal scan from the intense Mn  $2p_{3/2}$  core-level is not presented here, although for  $\theta=45^\circ$  it shows good agreement with the O  $1s$  curve of Fig. 6, and a similar anisotropy.

Figure 7 shows much more surface-sensitive azimuthal scans involving either grazing emission at high kinetic energies (O  $1s$  and Mn  $2p_{3/2}$  with Al  $K\alpha$  excitation) or a higher angle of takeoff of  $45^\circ$  but lower kinetic energies for which the surface sensitivity will be essentially equal to those in our SPPD experiments (Mn  $3p$  and Mn  $3s$  with Mo  $M\zeta$  excitation). Since the majority of the photoelectrons in this work will be at only about 100 eV, and thus rather near the minimum in the electron mean free path, it is important to verify that the first few surface layers are also very well ordered. Both the grazing-emission scans and the low-energy scans should probe this region. The high-energy O  $1s$  and Mn  $2p_{3/2}$  scans of Fig. 7(a) at a grazing angle of  $10^\circ$  again show the four-fold symmetry of the lattice (cf. similar behavior of the data at  $\theta=45^\circ$  in Fig. 6). The forms of these two high-energy curves also are substantially different, although both share a rather high anisotropy of 40% that is not much lower than that at the more bulk sensitive  $45^\circ$  angle of Fig. 6. In Fig. 7(b), low-energy scans of Mn  $3p$  and  $3s$  intensity at  $\theta=45^\circ$  also exhibit a four-fold symmetric curve with anisotropies of 44% that are almost as high as those of the data in Fig. 6. Taken together with the other surface analytical information presented above, there is thus no doubt that our measurements were performed on a clean, well-ordered surface of MnO(001).

### B. Observation of spin-polarized photoelectron diffraction effects

In now attempting to observe SPPD effects, we are concerned not only with surface structural order but also with magnetic order. The nature of the type-II magnetic order in MnO will cause a reduced symmetry at the surface due to the presence of ferromagnetically coupled spins in alternating  $\{111\}$  planes.<sup>9</sup> Two representative planes from the set of eight possible with all sign permutations of  $\{111\}$  are shown in Fig. 8, where only the Mn ions are shown for simplicity. A consideration of the symmetry of the scattering of Mn photoelectrons in leaving these eight distinct magnetic domains shows that they can be reduced to only the two representative ones shown in Fig. 8 for the measurements and theoretical simulations in the  $\phi=0^\circ$  or (010) plane to be discussed here. (This reduction was verified in SPPD diffraction calculations in which all domains were considered explicitly.) Due to the energy degeneracy of these domains and the presence of a certain number of defects on the surface, we would thus *a priori* expect to sample an approximately equal mixture of these two representative domains. In view of the presence of these domains, our SPPD measurements were first carried out along the surface normal

or [001] direction, since this direction implies in either domain an antiferromagnetic (AF) array of Mn scatterers with O atoms in between them. This geometry is illustrated in Fig. 8. By contrast, if we look along the [101] direction ( $\theta=45^\circ$ ,  $\phi=0^\circ$ ), a clear difference in the magnetic scattering is seen between the two domains. In domain I, the Mn spins are AF, and in domain II, they are ferromagnetic (F). All of the results to be presented here will consist of data obtained in the  $\phi=0^\circ$  plane (see the dashed curve in Fig. 8), and the two domain types will finally be assumed to be equal in probability in our later theoretical analysis.

We now consider the variation of the relative intensities of the spin-resolved Mn  $3s$  multiplet peaks that are indicated by  $^5S$  (spin-up) and  $^7S$  (spin-down) in Fig. 2 in an attempt to observe spin-dependent diffraction effects. Such  $3s$  spectra were taken with Mo  $M\zeta$  excitation along the [001] direction and over a temperature range from 70 to 750 K. Two spectra at 329 and 691 K that were part of the raw data from one series are shown in Fig. 9(a). The only normalization done to these data is to require

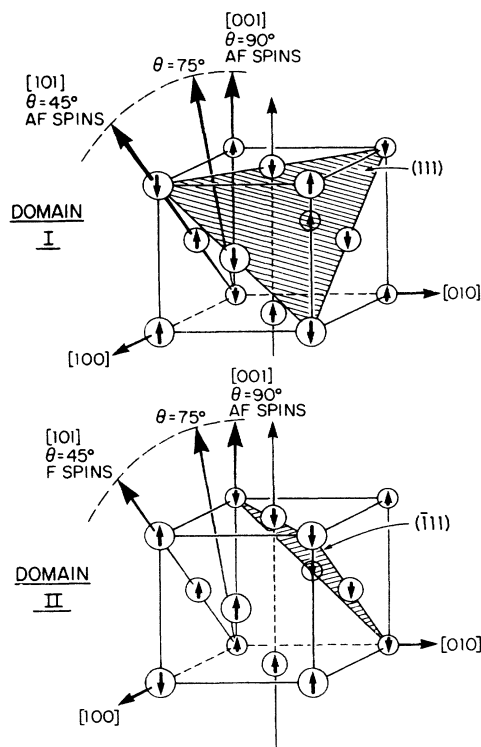


FIG. 8. The structural and magnetic order of the  $Mn^{2+}$  ions in MnO(001) below  $T_N$ . The dashed arcs show the (010) plane in which the experimental results were obtained. Also indicated are the two representative magnetic domains involved when scanning the polar angle in this plane. The difference between the two domains becomes obvious by noting that, for emission along  $\theta=45^\circ$  or [101], domain I has spins aligned in an antiferromagnetic fashion, while for this same direction domain II has spins aligned in a ferromagnetic fashion. Domain II is obtained from a simple  $90^\circ$  rotation around [001] of Domain I. [Since the magnetic moments lie in the  $\{111\}$  planes for MnO, the direction of the arrows in the figure should only be interpreted as illustrating parallel or antiparallel spin arrangements.]

the two  ${}^7S$  peaks to have the same overall height. (Comparing absolute intensities in raw data from one temperature run to another was not possible due to variations in both the Mo  $M\zeta$  x-ray flux and the bremsstrahlung-produced electron background with time.) Note the excellent matching of the electron backgrounds for the two normalized curves at the left and right ends of the spectra. The only difference between the two curves is an unambiguous decrease in the relative intensity of the  ${}^5S$  peak as temperature is increased from 329 to 691 K. The raw data were further analyzed by subtracting a linear background and applying a three-point smoothing to the spectrum. Figure 9(b) displays eight spectra from this refined data over the temperature range from 238 to 750 K. These curves show a clear and systematic trend for the  ${}^5S$  peak to decrease in relative intensity as temperature is increased. Closer inspection of these curves shows that the rate of change of this relative intensity is most rapid between  $\approx 530$  and  $\approx 560$  K.

In order to more quantitatively measure such changes in spin-up to spin-down relative intensities, we follow the same procedure as Sinkovic, Hermsmeier, and Fadley<sup>3</sup> and define a spin asymmetry that goes to zero for the

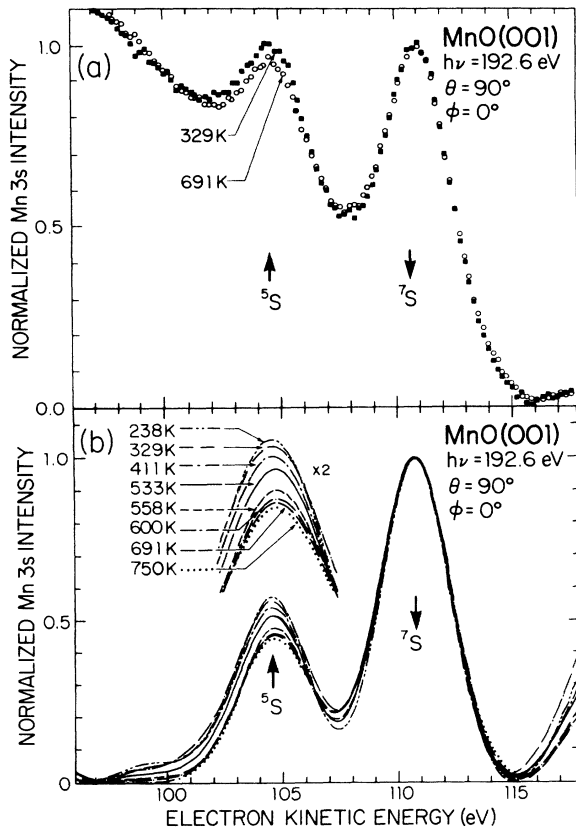


FIG. 9. The Mo  $M\zeta$ -excited spin-resolved  ${}^5S(1)$  and  ${}^7S$  peaks of the Mn 3s multiplet are shown for normal emission. A change in the  ${}^5S$ : ${}^7S$  intensity ratio as a function of temperature can clearly be seen, even in the raw data of (a) from which no background has been subtracted. In (b), curves from a larger number of temperature steps that have been smoothed and background-subtracted illustrate the systematics of the ratio variation.

highest temperature of a given scan. An accurate measurement of the intensities from the raw data of both the  ${}^5S$  and  ${}^7S$  peaks is made using a least-squares fit of two Gaussian functions riding on a linear background. From these intensities the experimental 3s spin asymmetry is calculated from the intensity ratio  $R = {}^5S$  (spin-up) to  ${}^7S$  (spin-down) at different temperature and the following equation:

$$S_{\text{expt}}(\text{LT}) = 100[(R_{\text{LT}} - R_{\text{HT}})/R_{\text{HT}}] \% , \quad (1)$$

where  $R_{\text{HT}}$  represents the  ${}^5S$ : ${}^7S$  intensity ratio for the highest-temperature data point in the series (assumed to be in the fully disordered or paramagnetic limit), and  $R_{\text{LT}}$  represents the same ratio for any lower-temperature data point below  $R_{\text{HT}}$ . (This equation is completely equivalent to the definition of  $S_{\text{expt}}$  found in Ref. 3). The spin asymmetries resulting from the series of Fig. 9(b) are plotted as a function of temperature in Fig. 10. The data shown here were scanned from high to low temperature, with a full return to the starting temperature at the end of the run, as shown by the open square. There is clearly very good reproducibility of these values and no indication that the properties of the sample changed during the series. There is a distinct step in  $S_{\text{expt}}$  at about 540 K, where it drops by approximately 10% over an interval of only 40 K. This step thus occurs at a temperature considerably above  $T_N$ , at approximately  $4.5T_N$ . These results are thus qualitatively similar to those from the previous SPPD study of  $\text{KMnF}_3$ ,<sup>3</sup> which also show a step in  $S_{\text{expt}}$  of 10–15% in magnitude at a temperature of  $2.7T_N$ . To verify the effect for the present case, we have repeated the full scan six times, and also made several

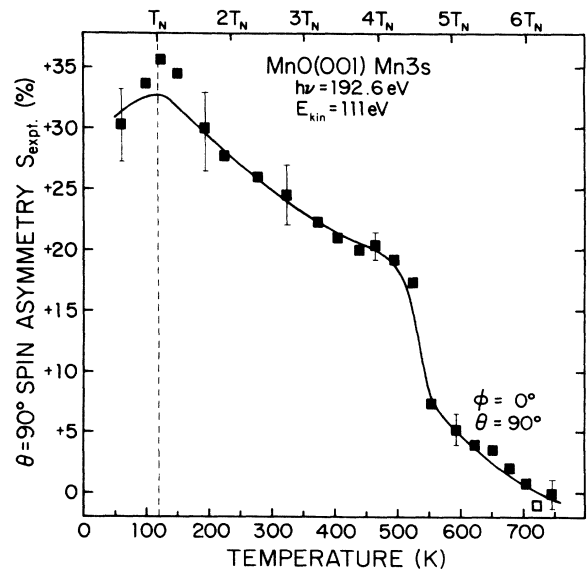


FIG. 10. Mn 3s experimental spin asymmetries  $S_{\text{expt}}$  with Mo  $M\zeta$  excitation are plotted as a function of temperature for  $\theta = 90^\circ$ . The temperature range covered is from  $\approx 50^\circ$  below  $T_N$  to  $\approx 620^\circ$  above it. Three features of the plot are apparent: the sharp step at  $\approx 530$  K labeled  $T_{\text{SR}}$ , the weak peak at  $T_N$ , and the relatively constant and gentle slope of the curve above and below  $T_{\text{SR}}$ .

quick jumps between temperatures just above and just below the step region (that is, between 490 and 630 K). The sample surface was also cleaned and reannealed before each series. The abrupt change in  $S_{\text{expt}}$  was fully reproducible and its maximum slope point was always within a  $30^\circ$  span in temperature centered at 540 K. Moreover, the temperature scans were also made in both directions, and no evidence of significant hysteresis in the step was noticed.

We have also investigated the directional dependence of this step in the spin asymmetry for Mn 3s by performing a similar variable-temperature study at a polar angle  $15^\circ$  off-normal in the (010) plane, indicated in Fig. 8 as  $\theta=75^\circ$  and  $\phi=0^\circ$ . As with the previous  $\theta=90^\circ$  emission direction, these data also produced a spin-asymmetry curve with a steep slope at very nearly the same temperature previously seen in Fig. 10, and the two separate curves are shown together in Fig. 11(b). For  $\theta=90^\circ$ ,  $S_{\text{expt}}$

is *positive* at low temperatures and there is a step  $\Delta S_{\text{expt}}$  of about  $-11\%$  centered at 540 K; for  $\theta=75^\circ$ ,  $S_{\text{expt}}$  is *negative* and a more gradual transition with maximum slope at 520 K and a  $\Delta S_{\text{expt}}$  of about  $+15\%$  is seen. (From our definition,  $S_{\text{expt}}$  must be zero for the highest temperature studied, and thus the general slope of the curve and the sign of  $\Delta S_{\text{expt}}$  must be opposite to the sign of  $S_{\text{expt}}$  at low temperatures.) Thus, the apparent transition temperature as judged from these two very reproducible curves is  $530 \pm 20$  K or approximately  $4.5T_N$ .

As noted previously, our results up to this point are qualitatively similar to those from a prior SPDD study of Mn 3s emission from  $\text{KMnF}_3$ ,<sup>3</sup> although there are also some important differences. Two of the temperature scans in the  $\text{KMnF}_3$  study for directions  $9^\circ$  apart are shown in Fig. 11(a). The overall changes in  $S_{\text{expt}}$  for MnO over the full temperature range studied are larger at about 25–30%, but the changes just around the transition region are comparable at 10–15%. Both curves shown for  $\text{KMnF}_3$  exhibit a *negative*  $S_{\text{expt}}$  and thus positive  $\Delta S_{\text{expt}}$  for the transition [note the opposite sense of the scale in Fig. 11(a) compared to those in 11(b)], although the step is increased in magnitude from 10% to 17% in rotating  $9^\circ$  away from the [001] direction. MnO shows a similar sensitivity to direction, but differs from  $\text{KMnF}_3$  in showing a dramatic change in the sign of the spin asymmetry with only a small rotation ( $15^\circ$ ) away from the [001] direction. Overall, the change in  $\Delta S_{\text{expt}}$  for MnO is from about  $-11\%$  along [001] to about  $+16\%$  at  $\theta=75^\circ$ , for a large net effect of 27% in the relative intensities of the spin-up and spin-down peaks. Other directions in the  $\phi=0^\circ$  plane also were studied and found to yield different  $\Delta S_{\text{expt}}$  values of  $\approx +8\%$  for  $\theta=82^\circ$  and a very small  $\approx +3\%$  for  $\theta=45^\circ$ . This sensitivity to direction for both  $\text{KMnF}_3$  and MnO is exactly what is expected for the case of spin-dependent scattering and diffraction processes,<sup>2</sup> although we consider several other possible explanations for these effects below.

Beyond changing direction and temperature, we also have searched for spin-dependent scattering effects in another spectral region: that of the Mn 3p multiplet. Here, 3p emission from  $\text{Mn}^{2+}$  leads to similar multiplet splittings and analogous  $^5P$  and  $^7P$  final states that should correspond to a high degree of spin-up and spin-down polarization, respectively.<sup>11–16</sup> The 3p spectral region is shown in both Figs. 2 and 12(a). The origin of these splittings again lies in the exchange interaction, but for such non-s emission, Coulomb interactions, as well as spin-orbit, crystal-field, and correlation effects, also must be taken into account in predicting such spectra.<sup>11,40</sup> These more complex interactions may cause additional spin mixing in the final states, thus leading to a lower degree of spin polarization, but we nonetheless expect a significant degree of polarization for the strongest  $^5P$  and  $^7P$  peaks that should be of the same sense as that in the  $^7S$  and  $^5S$  peaks. This is indicated in Fig. 12(a). Two recent studies have helped to further establish the spin-resolved nature of the 3p multiplet. The first work compared gas-phase Mn 3p data from atomic Mn to that of solid  $\text{MnO}$ ,<sup>16(a)</sup> and showed a high degree of similarity between atom and solid that indicates a strongly intraatomic ori-

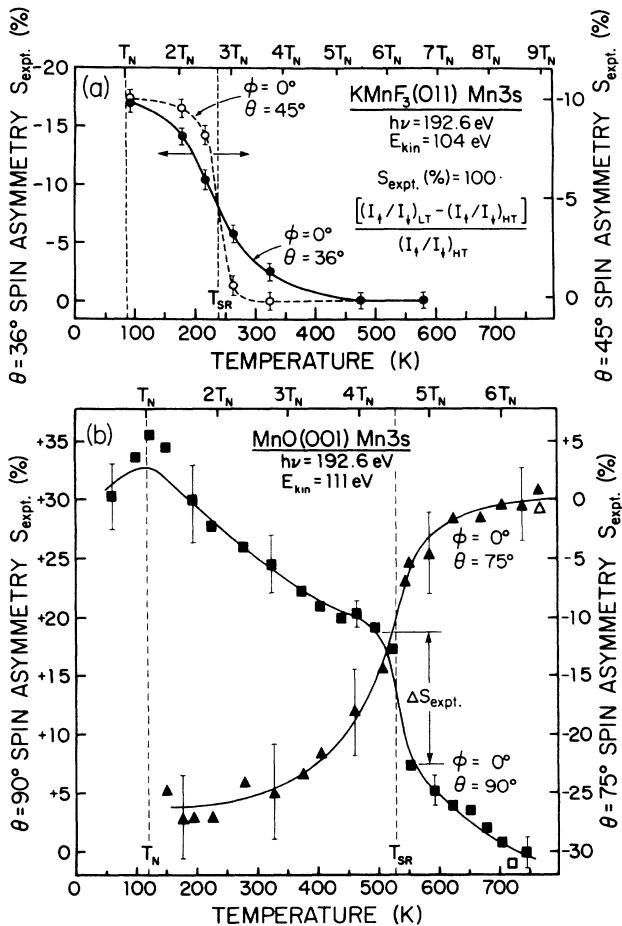


FIG. 11. The temperature dependence of Mn 3s spin asymmetries  $S_{\text{expt}}$  is shown for the two different systems studied to date and for several directions of emission. (a) Summary of the first observations of SPDD made for  $\text{KMnF}_3(001)$  by Sinkovic, Hermsmeier, and Fadley (Ref. 3). Emission along two different directions is shown, both of which gave a negative  $S_{\text{expt}}$  and positive steps at  $T_{\text{SR}}$ . (b) Analogous curves for  $\text{MnO}(001)$  for which both positive and negative  $S_{\text{expt}}$  values and steps are seen. Note the different directions of the scales in (a) and (b), and the 30% shift of the scales for the two curves in (b).

gin of the  $3p$  splittings in such ionic compounds. Thus, crystal-field effects and final-state extra-atomic screening do not significantly perturb the basically intra-atomic splittings observed. The second, a spin-resolved photoemission study with an external spin detector by Carbone and Kisker,<sup>41(a)</sup> directly measured the spin polarization of the Fe  $3p$  spectrum from metallic Fe and found a negative (spin-down) polarization of about  $-20\%$  on the low-binding-energy side of the peak and a positive (spin-up) polarization of  $+30\%$  on the high-binding-energy side. These results have recently been confirmed by Sinovic with better statistics.<sup>41(b)</sup> Although iron is a much more complex metallic system for which the multiplets are less well resolved, the directions of the polarizations found and their rather high magnitudes are qualitatively

consistent with the spin polarizations expected in the much more widely split Mn  $3p$  multiplet shown in Fig. 12(a).

We have thus made similar temperature-dependent measurements of the Mn  $3p$  spectrum for normal emission from MnO (001). Figure 12(a) is analogous to Fig. 9(b) in comparing two spectra with a linear background subtracted. These were obtained at temperatures of 661 and 530 K that are, respectively, above and approximately at the transition temperature seen for Mn  $3s$ . These spectra are normalized to have the same height for the  $7P$  peak. The widths of the spectra shown also span the Mn  $3s$  doublet considered previously. It is here striking that this normalization on  $7P$  also effectively yields a normalization on  $7S$ , and that both the  $5P$  and  $5S$  peaks show a similar decrease in relative intensity as temperature is increased. Thus, the two spin-up peaks exhibit parallel trends as measured against their spin-down partners in the multiplets. We have thus made a full temperature scan of the Mn  $3p$  spectrum for normal emission and determined the associated spin asymmetries from the values of  $R_{LT}$  and  $R_{HT}$  obtained and Eq. (1). Due to the more complex nature of the  $3p$  manifold (at least four  $5P$  peaks are seen in higher resolution spectra from atomic Mn,  $MnF_2$ , and MnO [Ref. 16(a)]) the intensities of the two peaks were obtained by simply taking peak heights after the removal of a linear background. The  $5P$  peak is rather broad and was always measured at 17.0 eV to the higher-binding-energy side of the  $7P$  peak. This peak-height method was checked against our Gaussian curve-fitting routine for the  $3s$  multiplet and found to be quite reliable when comparing systematic differences for well-behaved spectra such as these. The final Mn  $3p$  spin-asymmetry results are shown in Fig. 12(b), and they show very similar effects to those of Mn  $3s$  in Fig. 10: positive values of  $S_{\text{expt}}$ , a general negative slope in the curve in going from low to high temperatures that could in part be due to Debye-Waller effects, and a *negative* step in  $S_{\text{expt}}$  of about 10% which occurs with a maximum slope at about 540 K that is in complete agreement with the transition temperature seen for Mn  $3s$ .

A further interesting point in the normal-emission spin-asymmetry results for both  $3s$  and  $3p$  emission is that they show a very similar change in slope or probably a weak peak very close to the Néel temperature. Although the error bars on  $S_{\text{expt}}$  are larger in this minimum region of temperature due to the greater degree of charging present and lower stability of the cooling system, the features near  $T_N$  in the two curves are nonetheless strikingly similar. This is the first time that any effect has been seen in SPPD near  $T_N$ , and this is of interest since  $T_N$  is the long-range-order transition temperature and thus not necessarily a point at which a predominantly short-range probe like SPPD should detect anything. The fact that this feature is seen in both multiplets in spite of the much different energy spacings and intensity ratios involved further confirms that this effect is due to the disappearance of long-range antiferromagnetic order. A simple change in atomic positions, for example, through a slight contraction or expansion of the  $\{111\}$  interplanar distances upon losing long-range antiferro-

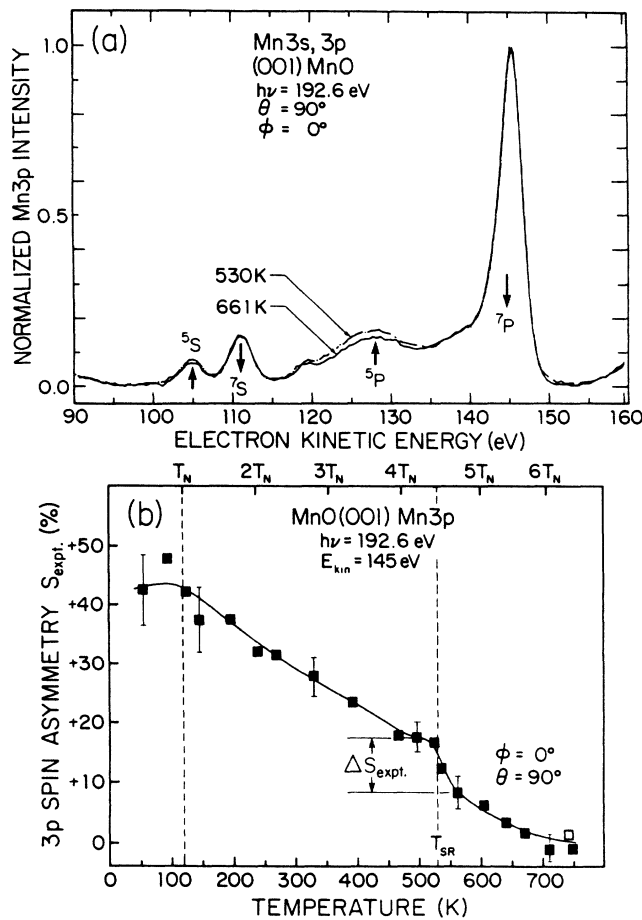


FIG. 12. (a) Mn  $3s$ - $3p$  spectra with linear background subtracted are compared for a temperature above  $T_{\text{SR}}$  and one approximately at  $T_{\text{SR}}$ . As in Fig. 9, there is evidence of a change in relative intensity of the Mn  $3s$  multiplet between the two curves. However, the same type of effect can also be seen in the  $5P$  and  $7P$  peaks of the Mn  $3p$  multiplet. By contrast, the relative intensities of the  $7P$  and  $7S$  peaks remain constant for the two temperatures, thus ruling out non-spin-dependent effects. In (b), the Mn  $3p$  spectra at several temperatures are translated into experimental spin asymmetries  $S_{\text{expt}}$  based upon the  $5P:7P$  ratio.  $S_{\text{expt}}$  shows a dependence on temperature that is very similar to that in Fig. 10.

magnetic order, would not be expected to affect the spin asymmetries of both multiplets in such a similar way. Therefore the very similar features seen in both the 3s and 3p data near  $T_N$  supports the idea that SPPD is also somewhat sensitive to the loss of long-range magnetic order as well. This longer-range sensitivity is not entirely surprising, since a recent study by Saiki *et al.*<sup>37</sup> of a strained oxide overlayer on Ni(001) using non-spin-resolved photoelectron diffraction shows that the fine structure in azimuthal scans is sensitive to the degree of strain and the placement of the atoms in spheres of neighbors farther away from the emitter, even though the gross features of the curves are primarily determined by the first few spheres. Similar azimuthal scans from  $c(2 \times 2)$  oxygen adsorbed on Ni(001) also are found to require clusters of 20–25 Å in radius in order to predict all of the fine structure in the diffraction patterns.<sup>18(e),37</sup> This longer-range aspect of SPPD indicated in the present data thus certainly warrants further study and verification.

These combined Mn 3s and Mn 3p results for MnO thus provide very convincing support for an interpretation of the high-temperature steps in spin asymmetry as being due to an abrupt reduction of short-range antiferromagnetic order. In Fig. 12(a), where the 3s and 3p multiplets appear in the same spectra, their combined energy range spans approximately 50 eV and the energy splitting between the  $^5P$  and the  $^7P$  peaks is approximately three times larger than the splitting for the  $^5S$  and  $^7S$ . The fact that two such different doublets at significantly different kinetic energies behave in such a similar way with respect to their quintet or septet ratios argues strongly for a spin-dependent scattering phenomenon in which the type of magnetic order changes suddenly at what has thus been termed the short-range-order transition temperature or  $T_{SR}$ .<sup>2</sup> Furthermore, if we note the energy separation between the  $^7P$  and  $^7S$  peaks and the constancy of their relative peak intensities above and below  $T_{SR}$  [see, e.g., Fig. 12(a)], it is extremely unlikely that any non-spin-specific type of diffraction effect, such as differential Debye-Waller damping due to the energy difference between the two peaks, could cause the observed temperature-dependent intensity changes in the  $^5S:^7S$  and  $^5P:^7P$  ratios and yet leave the  $^7S:^7P$  intensity ratio unaffected. Other possible spin-independent scattering effects will be discussed further below. The apparent ability of SPPD to detect longer-range magnetic order for both 3s and 3p emission in turn adds further credence to the idea that the steps at  $T_{SR}$  are due to the greater sensitivity of the technique to shorter-range order.

We now consider other possible causes of such an abrupt step in spin asymmetry to be certain that it is associated with spin-dependent effects in scattering. From our prior discussion of the cleanliness, stoichiometry, and degree of near-surface order of the MnO(001) surface, the origin of this step cannot be associated with impurities or surface disorder. However, there remain the possibilities of a bulk or surface structural phase transformation or some sort of less likely discontinuity in the differential Debye-Waller attenuations of the two peaks upon passing through the step. Figure 13 directly addresses these pos-

sibilities by comparing Mo  $M\zeta$ -excited Mn 3p- $^7P$  azimuthal scans at  $\theta=45^\circ$  that were taken in a quick sequence at temperatures below, above, and below the step in  $S_{\text{expt}}$  (cf. Fig. 10). The Mn 3p photoelectrons here have energies and thus inelastic attenuation lengths that are very close to those of the 3s spectra involved in Fig. 10; using a  $45^\circ$  takeoff angle also reduces the effective penetration depth (which is given by  $\Lambda_e \sin\theta$  if  $\Lambda_e$  is the electron inelastic attenuation length) for this scan to almost exactly what is expected for our Mn 3s data at normal emission. The very close similarity of the three curves in Fig. 13 shows no evidence for any near-surface structural change. The only observed effect is a small 3% decrease in the overall anisotropy with no change in the features in the scan, effects which can easily be explained by normal Debye-Waller attenuation with no discontinuity. We therefore conclude that the observed step in  $S_{\text{expt}}$  cannot be due to either a surface structural change or a discontinuous change in the Debye-Waller effects on the two peaks involved.

In order to also investigate the possible influences of charging and flood-gun effects, several studies were conducted with the flood gun *off*. Since the sample surface becomes fully conductive approximately  $80^\circ$  before this step region is reached (cf. Fig. 4), multiplet temperature-dependent scans were obtained over this region without the use of the flood gun and with no observed charging effects. The spin-asymmetry results showed no observ-

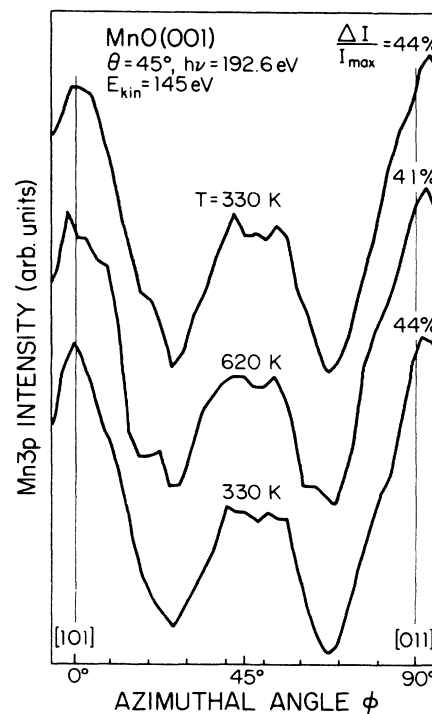


FIG. 13. Three azimuthal scans of Mn 3p intensity obtained with Mo  $M\zeta$  excitation at a polar angle of  $45^\circ$  which were run sequentially at 330, 620, and 330 K. These temperatures were chosen to be below and above the transition region at approximately 530 K seen in the Mn 3s spin asymmetries of Fig. 11(b). The overall anisotropy is given for each curve.

able difference from those using the flood gun. Moreover, as the temperature was decreased through the onset of the charging region (that is, below about 460 K) with the flood gun off, the spin asymmetries showed no step or otherwise anomalous behavior, even though there were progressive peak shifts to higher binding energies and increases in peak widths. Thus, charging is certainly not responsible for the step in spin asymmetry.

As a final aspect of our core-level data, we also consider the potential measurement of such SPPD effects at the much higher energies of  $\geq 1000$  eV that are typical of normal XPS measurements. Prior theoretical estimates of SPPD effects<sup>2</sup> indicate that the effects of exchange scattering on spin asymmetries should become negligibly small ( $< 1\%$ ) at such high energies. To assess this prediction, we have repeated the Mn 3s measurements discussed above using Al  $K\alpha$  radiation and a normal-emission geometry. These measurements spanned a less extensive temperature range, but still included  $T_{SR}$ . Using Al  $K\alpha$  excitation gives a well-resolved 3s multiplet with a good peak-to-background ratio, as seen in Fig. 2. A closeup of this multiplet is shown in Fig. 14(a), where the raw data for two temperatures of 728 and 514 K (i.e., above and just below  $T_{SR}$ ) are compared. The fact that no discernible change is found in the  $I(^5S)/I(^7S)$  intensity ratio between these two temperatures is in strong contrast to the analogous results with Mo  $M\zeta$  excitation in Fig. 12(a). Converting this Al  $K\alpha$  data into spin asymmetries in exactly the same way as for the Mo  $M\zeta$  data

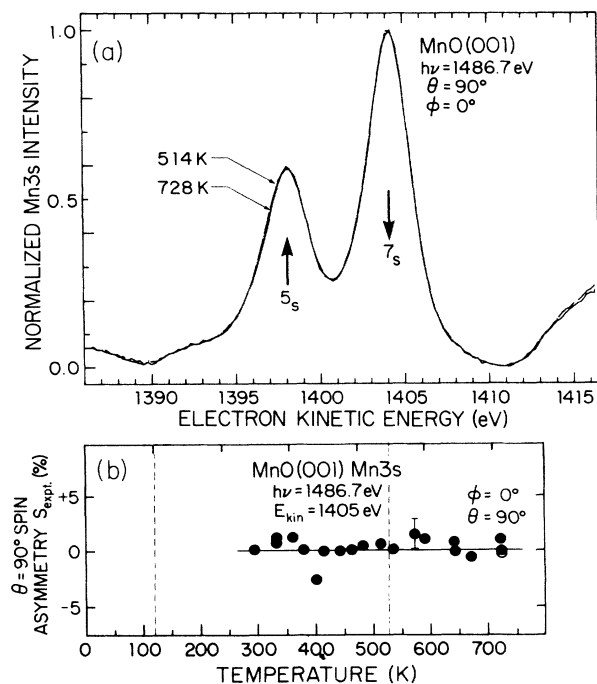


FIG. 14. (a) Raw data for the Al  $K\alpha$ -excited spin-resolved  $^5S$  and  $^7S$  peaks of the Mn 3s multiplet are shown for normal emission as in Fig. 9. However, unlike Fig. 9, there is no evidence of a relative change in intensity as a function of temperature. Spectra at several temperatures yield the experimental spin asymmetries plotted in (b); these data confirm that  $S_{\text{expt}}$  is constant with temperature.

above yields the results plotted in Fig. 14(b). Within the scatter of the data of about  $\pm 1.5\%$ , the spin asymmetry is constant over the full temperature range scanned. These results thus further support the interpretation of the steps in  $S_{\text{expt}}$  at lower kinetic energies as being due to a short-range magnetic order transition. They also make it clear that, in order to have observable effects, SPPD experiments will require the use of lower-energy excitation sources such that the electrons leave the specimen with only about 50–200 eV of kinetic energy.

Based upon this core-level data for Mn 3s and 3p emission with both Mo  $M\zeta$  and Al  $K\alpha$  excitation, we are thus led to the same conclusion as Sinkovic, Hermsmeier, and Fadley<sup>3</sup> in their prior study of  $\text{KMnF}_3$ : that the step in spin asymmetry is caused by a rather sharp decrease in the degree of short-range spin order as temperature is increased. This model<sup>2,3</sup> thus assumes that the sudden drop in  $S_{\text{expt}}$  is due to an abrupt, spin-dependent, change in the scattering potential of the crystal. This change in turn arises when the magnetic moments of near-neighbor  $\text{Mn}^{2+}$  ions around a given emitter realign from what is probably antiferromagnetic order below  $T_{SR}$  to a state in which each site approaches the “paramagnetic” limit of having an equal probability of being spin up or spin down, regardless of its position with respect to the emitter. (This is equivalent to the near-neighbor spin-spin correlation functions going to zero above  $T_{SR}$ .) It is not surprising that some SRMO persists in MnO at high temperature, since neutron-scattering measurements already indicate its presence above  $T_N$ ,<sup>9</sup> and simple mean-field theoretical models also predict its presence.<sup>24</sup> What is surprising is that our results indicate that this SRMO disappears very suddenly at  $T_{SR}$ , an effect which is not predicted by any current model of the short-range spin-spin correlation function of which we are aware.<sup>24–26</sup> Mean-field approaches in general predict a monotonic decay of the pair-correlation functions, with no abrupt transitions,<sup>24</sup> and this has been verified in model calculations based upon the Ising model for  $\text{KMnF}_3$  by Moran-Lopez and Sanchez.<sup>25</sup> Adding in the effects of more neighbors and accounting properly for the frustration that is inherent in antiferromagnetic order for these systems has been found by Noguera and Nigel<sup>26</sup> to produce very small steps in the correlation functions at high temperature, but these are not of sufficient magnitude, nor at the proper temperature, to directly explain our data. It remains to be seen whether more exact approaches using more complex interaction Hamiltonians and/or large-cluster Monte Carlo simulations<sup>42</sup> will yield such a high-temperature transition. We stress that SPPD measurements emphasize near-neighbor interactions over the first four to five spheres of neighbors, and that they sense the local spin environment on a very-short-time scale of  $\approx 10^{-16}$ – $10^{-17}$  sec. Thus, the technique provides a short-range “snapshot” of spin configurations as averaged over all emitters at a given temperature.

As a consequence of the short-range sensitivity of photoelectron diffraction in general and SPPD in particular, the long-range magnetic order transition at  $T_N$  should have only a small effect on such measurements. This is consistent with the rather weak peaks observed near  $T_N$

in Figs. 11(b) and 12(b). Unfortunately, studying these peaks more quantitatively was not possible due to the extreme sample charging problems encountered at these low temperatures. Finally, the more gentle slopes of  $S_{\text{expt}}$  above and below  $T_{\text{SR}}$  also may be dependent on changes in magnetic order, since the spin-spin correlation function is expected to show a monotonic reduction in magnitude with increase in temperature.<sup>24–26</sup> As noted previously, differential Debye-Waller effects for the two peaks involved, which are also expected to have a simple monotonic form,<sup>43,44</sup> also may contribute to these slopes, making it difficult to distinguish between Debye-Waller and true spin-asymmetry effects in these temperature ranges.

### C. Temperature effects on valence-band spectra

As a final aspect of our data, it is also of interest to consider the behavior of the spin-up Mn 3*d* valence electrons which give rise to the magnetism in the sample and the core multiplets themselves. In fact, the constancy of the multiplet peak separations and general relative intensities (with the exception of small SPPD effects) in all of our data indicate that these valence electrons are coupled to the same  $S = \frac{5}{2}$  localized moment over the full range of temperature studied, at least as viewed in the core-hole final state of photoemission. We now ask whether there is any temperature dependence in the valence spectra.

As the first part of this data, temperature scans of Mo  $M\zeta$ -excited valence-band (VB) spectra over  $T_{\text{SR}}$  showed that, to within the rather low-energy resolution of these measurements [approximately 2.2-eV full width at half maximum (FWHM)], there was no change in the width or shape of the primary 3*d* peak upon passing through  $T_{\text{SR}}$ . These results are presented in Fig. 15(a), and they are compared to reference core-level 3*p* (<sup>7</sup>*P*) spectra at the same two temperatures in Fig. 15(b).

The second part of these results was motivated by a recent theoretical study of transition-metal monoxides and dihalides, including MnO, by Ojala and Terakura,<sup>45</sup> in which they predict a change in the density of states between the antiferromagnetic and the paramagnetic states; we have thus also monitored the valence-band spectrum of MnO(001) in crossing  $T_N$ . As shown in Fig. 15(c), there are no dramatic changes in the general shape of the *d*-band doublet (cf. similar doublet in Fig. 2), but there is a large 0.4-eV shift in the low-binding-energy edge so as to broaden the overall width for temperatures below  $T_N$ . Figure 15(d) confirms that this cannot be attributed to a charging effect or spurious resolution change since the core-level 3*p* (<sup>7</sup>*P*) peaks taken immediately before the respective VB curves in time show no measurable change in resolution. (The slightly higher background for the low-temperature 3*p* scan is largely due to the SPPD effect for the other <sup>5</sup>*P* peaks associated with the 3*p* manifold.)

This broadening of the valence bands below  $T_N$  is not the direction of effect predicted by theory,<sup>45</sup> but it does suggest a sensitivity of VB spectra to magnetic order that has not to our knowledge been observed before. The fact that the valence-band width shows more sensitivity to temperature over the long-range-order transition than over the short-range-order transition is also not surpris-

ing in view of the more extended nature of the valence states. These effects thus deserve more careful, higher resolution study with a range of excitation energies.

### D. SPPD: Comparison of experiment and theory

As a tractable first step toward a theory of SPPD effects, we consider the single-scattering cluster (SSC) model with spherical-wave (SW) scattering, as discussed in detail elsewhere for both the usual form of photoelectron diffraction<sup>18</sup> and spin-polarized photoelectron diffraction.<sup>2</sup> The generalization of the SSC-SW formalism to include spin effects consists first of simply keeping track of the spin of the photoelectron with respect to the unpaired 3*d* electrons of each magnetic scatterer. Then, if the photoelectron spin is parallel to that of a magnetically ordered scatterer ( $\uparrow\uparrow$  or  $\downarrow\downarrow$ , with the first spin orientation being that of the photoelectron and the second the scatterer spin), an exchange interaction with these unpaired *d* electrons is included in calculating the overall scattering potential and the scattering phase shifts. If the photoelectron spin is antiparallel to the unpaired spins of a scatterer ( $\uparrow\downarrow$  or  $\downarrow\uparrow$ , in the same notation), this exchange interaction is omitted. This spin-dependent scattering is modeled using a specially modified muffin-tin (MT) potential program that finally produces phase shifts  $\delta_1$  at the internal kinetic energy of the photoelectron of interest (i.e., at an energy equal to its external kinetic energy plus the inner potential). For treating the high-temperature paramagnetic limit, it can be shown [2(c)] that averaging over the spin configurations of the magnetic scatterers is accurately accounted for by using these scatterers the average of the appropriate spin-parallel and spin-antiparallel phase shifts as defined above (that is, either  $[\delta_1(\uparrow\uparrow) + \delta_1(\uparrow\downarrow)]/2$  or  $[\delta_1(\downarrow\downarrow) + \delta_1(\downarrow\uparrow)]/2$ ). These two average quantities are close to one another, but are not exactly equal because of the slight energy difference between the spin-up and spin-down photoelectrons in the multiplet. As noted before, we will make use of two different approaches based upon density-functional theory for treating the exchange interaction: the Dirac-Hara (DH) and Kohn-Sham (KS) approximations (cf. Fig. 6). The DH form is expected to be somewhat more appropriate to the scattering of high-energy free electrons.<sup>6,19</sup> We will not attempt to describe in detail the statistical mechanics of the transition at  $T_{\text{SR}}$ , but simply treat the two extremes by assuming that SPPD can be described by either a fully ordered antiferromagnetic lattice for  $T < T_{\text{SR}}$  or a fully disordered paramagnetic lattice for  $T > T_{\text{SR}}$ . We justify a fully ordered system even in the SRMO regime by again pointing out that SPPD is primarily sensitive to the first four to five near-neighbor spheres. Calculating the  ${}^5S:7S$  intensity ratio for temperatures just above and just below  $T_{\text{SR}}$  then yields the ratios appropriate for determining the change in the Mn 3*s* spin asymmetry associated with the transition from Eq. (1). This type of theoretical treatment is discussed in detail elsewhere by Sinkovic *et al.*<sup>2(a),2(b)</sup> This model may require corrections due to multiple scattering to make it fully quantitative for predicting SPPD effects, especially in view of the low kinetic

energies of approximately 100 eV involved; in fact, Friedman *et al.*<sup>2(d)</sup> have, in fact, recently carried out multiple-scattering calculations of this type. But our intent here is to determine the degree to which a simple picture can at least qualitatively predict our experimental observations.

There are several nonstructural inputs for these calculations beyond the scattering phase shifts for  $\text{Mn}^{2+}$  and

$\text{O}^{2-}$  with the various energies and relative spin orientations involved. The touching MT radii used for  $\text{Mn}^{2+}$  and  $\text{O}^{2-}$  were 1.833 and 2.730 bohr, respectively. The other parameters chosen were based on a comparison of experiment and theory for non-spin-polarized results, but are all within the range of what would in any case be choices based upon independent literature values. These parameters were as follows: (1) an inner potential  $V_0$  of

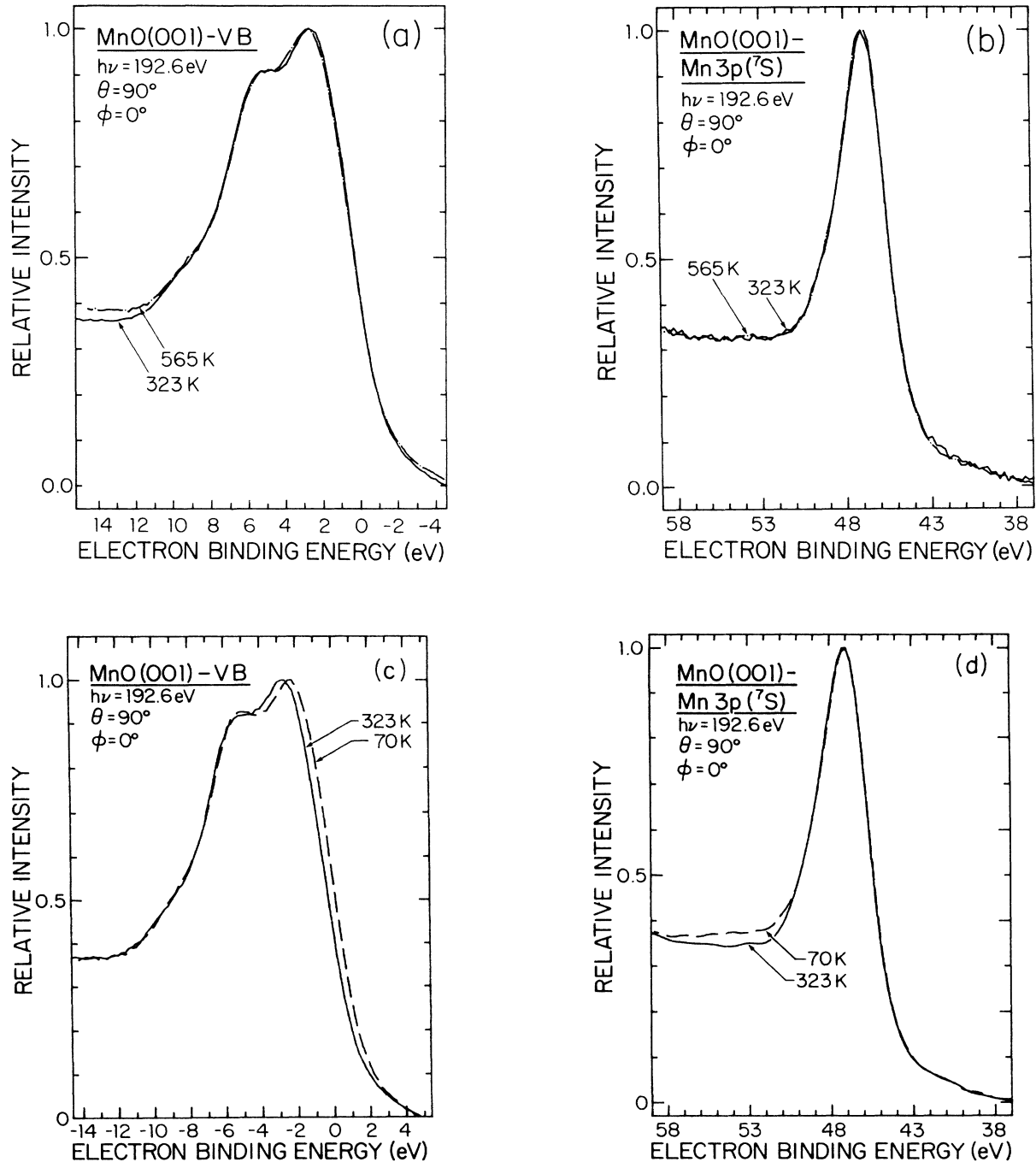


FIG. 15. (a) The alteration of the MnO(001) valence band (VB) which occurs on going from below to above the short-range magnetic order temperature  $T_{SR}$ . This data was taken at normal emission using Mo  $M\zeta$  radiation. (b) Mn 3p ( ${}^7P$ ) core peak spectra taken at the same time as such VB curve in (a) as a resolution check. (c) As (a), but for temperatures above and below the long-range magnetic order temperature  $T_N$ . (d) As (b), but for temperatures above and below  $T_N$ .

25 V which is in reasonable agreement with theoretical calculations,<sup>46</sup> (2) an electron attenuation length  $\Lambda_e$  of 5.0 Å for both spin-up and spin-down electrons with an average internal kinetic energy of 128 eV,<sup>47</sup> (3) an angular broadening in the analyzer of  $\pm 3^\circ$ , and (4) a temperature-dependent three-dimensional mean-squared displacement  $\langle U^2 \rangle$  for including Debye-Waller effects of  $0.00322 \text{ \AA}^2$  at ambient temperature that corresponds to an average Debye temperature for  $\text{Mn}^{2+}$  and  $\text{O}^{2-}$  vibrations of  $\approx 500 \text{ K}$ .<sup>44,48</sup>

As a first test of our theoretical model for predicting such low-energy experimental results, we compare experiment and theory for azimuthal scans of the *total* Mn 3s multiplet intensity, i.e., the sum of both the  $^5S$  and  $^7S$  peaks. In Fig. 16, the experimental curve from the bottom of Fig. 7 is compared to two theoretical curves, one using KS exchange and the other using DH exchange. Due to the relatively weak 3s signal and resultant high noise level, the main structures to be considered are the two peaks at  $\phi=0^\circ$  and  $90^\circ$  and the broad dip between them centered at  $\phi=45^\circ$ . Both the KS and DH curves reproduce the broad dip, and they agree with experiment in showing the highest intensity features near  $0^\circ$  and  $90^\circ$ . The only discrepancy is the sharp dip at  $\phi=0^\circ$  and  $90^\circ$  which occurs for emission along high-density [101] atomic rows of Mn and O ions (cf. Fig. 8); this disagreement is less pronounced for the KS curve. This discrepancy is thus in a direction in which there are numerous scatterers, including the nearest neighbors to a given Mn emitter, and it may suggest the need for a multiple-scattering (MS) approach at such low kinetic energy.<sup>2(d)</sup> Nonetheless, the general shape of the experimental curve

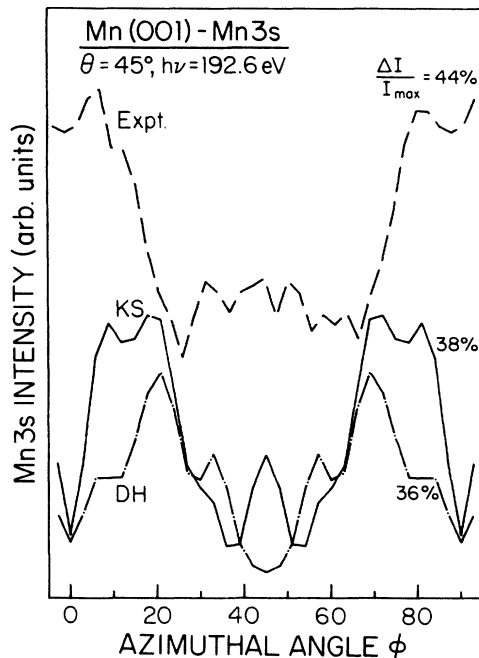


FIG. 16. Comparison of experiment to theory for a  $\text{MoM}\zeta$ -excited Mn 3s azimuthal scan. There are two single-scattering spherical-wave cluster theory curves differing only by the exchange potential used. These are designated by DH for Dirac-Hara and KS for Kohn-Sham.

is reproduced reasonably well by theory and we expect it to give us some useful insight into the qualitative systematics of SPPD even if it is not fully quantitative at such low energies.

In order to explore the sensitivity of our spin-polarized calculations to the nonstructural parameters discussed previously, we show in Figs. 17 and 18 a series of theoretical spin asymmetries as a function of polar angle for scans in the  $\phi=0^\circ$  plane of our experiments shown in Fig. 8. For simplicity, we consider for now only emission from MnO with AF order of the type in domain I. Each curve shown retains the parameters given in Fig. 17(a) except for the change indicated immediately above the curve. Note that the DH curves generally give much smaller amplitudes and are usually multiplied by 3 to permit easier comparison to the KS curves. The general similarity of all of the curves in Fig. 17 indicates that these results are rather insensitive to the precise choices of the parameters involved. Specifically, increasing  $V_0$  from 15 to 25 eV primarily shifts features to lower polar angles due to refraction effects. Omitting angular broadening shows more fine structure as expected, but leaves the gross form of all features unchanged. Raising or lowering the electron mean free path by a very

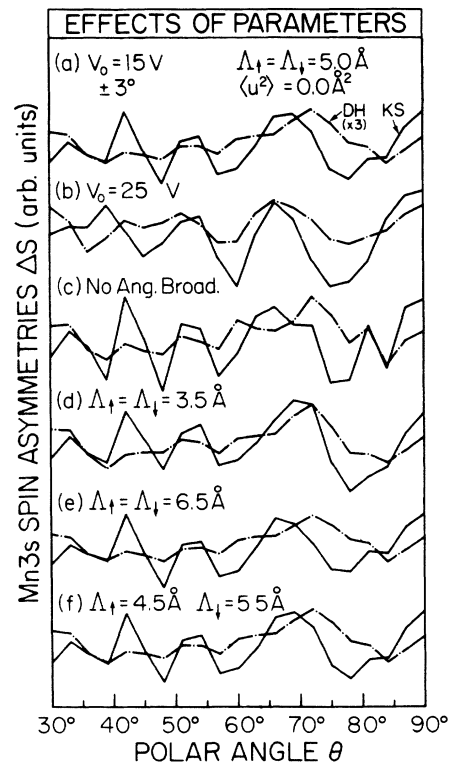


FIG. 17. Study of the sensitivity of theoretical polar scans of spin asymmetry for the spin order of domain I in Fig. 8 to the choice of several nonstructural input parameters, as indicated on the curves. With (a) as a reference, all parameters were kept constant except for those indicated above curves (b)–(f). The inner potential, degree of angular broadening, and electron mean free paths are varied. The Dirac-Hara curves are multiplied by a factor of 3 for ease of comparison.

significant  $\pm 30\%$  also causes very little change in the predicted spin asymmetries. And finally, letting the spin-up and spin-down electrons have different mean free paths that are  $\pm 10\%$  with respect to the initial  $5.0 \text{ \AA}$  (an extreme change compared to prior estimates of this difference<sup>6</sup>) also is found to make almost negligible changes in the curves; thus, differential spin-dependent inelastic scattering does not appear to be a significant cause of the SPPD effects of the order of 10% that are seen experimentally. In Fig. 18, we consider the effect of temperature through Debye-Waller effects. These results by contrast show greater sensitivity to the nature of the modeling used. The curves in (a) represent a rigid-lattice model where no vibrations are allowed. Both the KS and DH (again usually multiplied by 3) results exhibit the same general features, especially for the higher polar angles of interest to us experimentally. In (b), for which the  $\langle U^2 \rangle$  values of low and high temperatures are both set equal to the ambient temperature value, there are practically no observable differences relative to (a). In (c), where the vibrational contributions to the paramagnetic calculation at HT is now taken to be 560 K, i.e., just above  $T_{SR}$ , and the vibrational contributions to the anti-ferromagnetic state at LT is taken to be 490 K and just

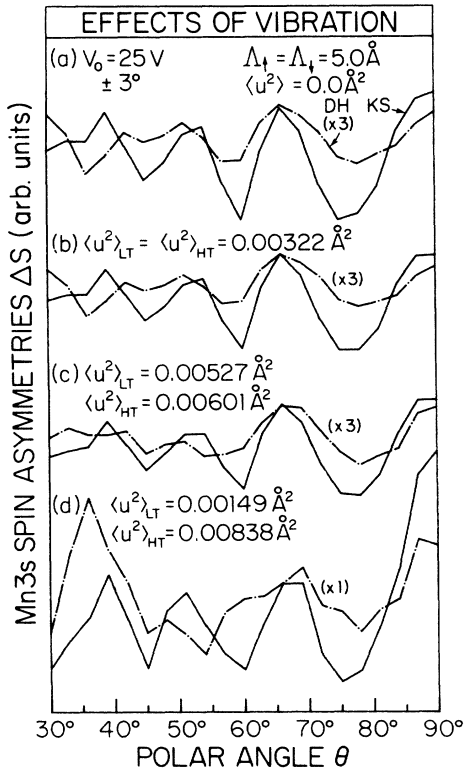


FIG. 18. As Fig. 17, with a different reference in (a). Here, the dependence of the theoretical spin asymmetries on Debye-Waller effects is considered by varying the one-dimensional mean-squared displacements  $\langle U^2 \rangle$ : (a) a rigid lattice where no vibrations are allowed; (b) vibrations corresponding to a temperature of 300 K; (c) vibrations corresponding to temperatures just above (560 K) and just below (490 K)  $T_{SR}$ ; and (d) vibrations corresponding to temperatures well above (780 K) and well below (77 K)  $T_{SR}$ . Only in the last case are significant differences seen with respect to (a).

below  $T_{SR}$ , a very small change begins to appear. This method of calculation in fact represents the most realistic approach to predicting the step in anisotropy as measured just across  $T_{SR}$ , and it suggests that the correct inclusion of vibrational effects is *not* crucial. For the extreme case shown in (d), however, this is not the case. Here, HT equal to 780 K and LT equal to 77 K are chosen to represent the extreme temperatures encountered in our experiment, and they show the unexpected result that the DH curve is increased in amplitude relative to the KS curve by a factor of approximately 3, thus not needing for this case to be multiplied by 3 to better match the KS results. The form of the DH curve also changes somewhat during this amplification. The KS curve also shows a net increase in spin asymmetry for this case, but still exhibits the same general form as before. We therefore conclude that such Debye-Waller effects may affect the predicted spin asymmetries over extreme temperature ranges, but not over the  $20^\circ$ – $40^\circ$  span centered at  $T_{SR}$  over which the step in  $S_{\text{expt}}$  occurs.

We now compare these experimental results for the step in  $S_{\text{expt}}$  at  $T_{SR}$  to theoretical predictions based upon the set of nonstructural parameters introduced above. The two temperatures used to determine the low-temperature and high-temperature mean-squared vibrational displacements were 490 and 560 K and thus were identical to those used in determining the experimental step value. Figure 19 shows three sets of theoretical curves, one for antiferromagnetic orientation of the type in domain I, one for that in domain II (cf. Fig. 8), and one for the equally weighted sum of the two; all three sets have the same experimental points superimposed for comparative purposes. Theory and experiment are on the same scale, and are plotted with the sign of the overall spin asymmetry; thus the actual sign of the step in  $S$  or  $\Delta S$  in going from low to high temperature is the opposite of the values shown in the figure, as indicated on the ordinate label. The results with Dirac-Hara exchange from each set are again multiplied by 3 to better permit comparing features. Figure 19(a) for domain I shows very good agreement between theory and experiment for the KS curve, with prediction of the observed positive value at  $\theta = 90^\circ$  and the rapid change to negative values for the other three  $\theta$  values studied. There is even reasonable agreement for the magnitudes of the steps for all four points. The DH curve shows similar trends, but there is an underestimation of the observed SPPD magnitudes by a factor of 3 or more. (In general, the KS and DH curves are very similar in shape for all three sets of curves in this figure.) The agreement in Fig. 19(a) may be fortuitous, however, in view of the fact that we have no reason to expect our surface to be predominantly of domain I in magnetic order. In fact, the presence of surface defects such as the blemishes discussed in the experimental section might be expected to give rise to a roughly equal representation of eight distinct domains originating from the ferromagnetic (111) planes. As discussed previously, from the point of view of their effect on internally referenced spin-up to spin-down ratios in SPPD, domain I in Fig. 8 can be taken to represent four of these (111) domains and domain II to represent the other four. The

comparison of experiment and theory for domain II in Fig. 19(b) shows much poorer agreement and suggests that, based upon this first level of the theory of SPPD, domains of type II are minority constituents of our surface. Figure 19(c) shows the results of adding the two domains with equal weight, yielding what we would *a priori* estimate the surface to be. Although the fit with experiment is not as good as Fig. 19(a), it should be a more realistic comparison. Taking Fig. 19(c) then as the best representation of our theoretical predictions thus leads to the conclusion that some but not all of the experimental magnitudes and trends are predicted by the KS curve (and by the DH curve with a multiplication by 3). However, the important change of sign in the step of  $S_{\text{expt}}$  in going from  $\theta=90^\circ$  to  $\theta=75^\circ$  is not predicted by the summed KS curve; for this case, as noted above, the domain I results are in much better agreement with experiment.

Clearly, more experimental data is needed to establish the detailed form of such curves in temperature-dependent SPPD  $\theta$  scans, and the theory needs to be extended to include, for example, multiple-scattering (MS) effects that might be expected to come into play at such low energies. Moreover, preliminary results by Friedman *et al.*<sup>2(d)</sup> indicate that MS paths linking two Mn ions via a nearest-neighbor O ion may have a significant effect on

the predicted spin asymmetries. But it is, in any case, encouraging that the simple single-scattering theory we have used here is able to predict certain aspects of the experimental results, including approximately the correct magnitudes for the observed effects if the KS exchange is used. This degree of agreement provides a further point of support for the attribution of these steps to changes in the spin-dependent exchange-scattering environment around each  $\text{Mn}^{2+}$  emitter due to an abrupt change in the degree of short-range magnetic order. The fact that the DH exchange approximation so consistently underestimates the changes in spin asymmetry also raises the question of whether it similarly underestimates the strength of exchange scattering at such energies; other evidence for this type of inadequacy in DH exchange also exists.<sup>19</sup>

Finally, we consider whether the short-range-order transition observed here is limited to the surface layer of the material, which may have different ordering temperatures from the bulk, or represents a more bulklike property extending several layers inward from the surface. Our low-energy SPPD measurements are very surface sensitive and it is therefore not possible with complete certainty to rule out a surface-specific effect on SRMO. But there are a few aspects of our data that suggest an effect which penetrates inward by the order of the electron mean free path or at least a few monolayers. If the high-temperature transition were unique to the surface layer, it would nonetheless be expected that a few layers would be necessary for the electronic structure, and thus the temperature of this transition, to converge to bulk behavior.<sup>49</sup> If this were true, then additional steps or at least significant broadening would be expected in our temperature scans over the range between  $T_N$  and  $T_{\text{SR}}$ . The relatively sharp and single steps observed suggest that the first few layers are acting in concert to produce the observed changes in spin asymmetries. In addition, the theoretical modeling that we have just discussed has assumed that all layers contribute to the observed effects, and, even with the stronger KS exchange, is only just able to predict approximately the correct magnitudes of the steps. If the model were changed to involve only a single layer, the predicted effects would be significantly smaller than experiment.

#### IV. CONCLUSIONS

In conclusion, we have used core multiplet spectra as internally referenced sources of highly spin-polarized electrons. By the simple expedient of energy resolving these multiplets and without the need for an external spin detector, it has been possible to examine in detail a new type of high-temperature short-range magnetic order transition which for MnO occurs at a temperature  $T_{\text{SR}}$  of  $530 \pm 20$  K. The various angle and temperature scans of core spectra obtained in this study permit the more conclusive elimination of other possible nonmagnetic causes for the rather sharp changes in the spin-up to spin-down ratio (or equivalently in the spin asymmetry  $S_{\text{expt}}$ ) than has been possible in prior experimental studies<sup>3-5,27</sup> of such spin-polarized photoelectron diffraction (SPPD)

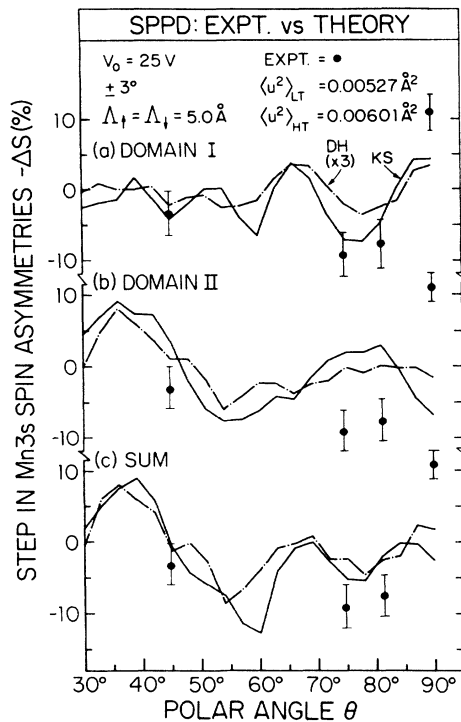


FIG. 19. Theoretical spin asymmetry steps on crossing  $T_{\text{SR}}$  are compared to the four corresponding experimental points from this study. Three pairs of theoretical curves are shown corresponding to (a) domain I, (b) domain II, and (c) the sum of domain I and domain II. All other nonstructural parameters were kept constant. Both the theory and the experimental are on the same vertical scale, although the Dirac-Hara curve is multiplied by 3 to facilitate comparing it to the Kohn-Sham curve in each case.

effects. In summary, these results show the following.

(i) A high degree of cleanliness, good stoichiometry, and high degree of crystalline order of the MnO(001) surface studied.

(ii) For emission at kinetic energies of approximately 100 eV, distinct steps of up to 10% in magnitude in  $S_{\text{expt}}$  at a temperature of  $T_{\text{SR}} = 4.5T_N$  for both Mn 3s and Mn 3p emission, and a high sensitivity of the step magnitude and sign to the direction of emission.

(iii) Qualitative agreement of these results with the prior study by Sinkovic, Hermsmeier, and Fadley<sup>3</sup> of Mn 3s spin asymmetries in  $\text{KMnF}_3$ , where steps of similar magnitude are seen at  $T_{\text{SR}} = 2.7T_N$ , and a similar sensitivity to the direction of emission was noted.

(iv) For emission at higher energies of approximately 1400 eV for which the spin-dependent aspects of electron scattering are expected to be much reduced, there is no evidence for a change in  $S_{\text{expt}}$ .

(v) A lack of any evidence for a surface structural phase transition occurring as  $T_{\text{SR}}$  is crossed.

(vi) The first observation of smaller effects on core spin asymmetries in crossing  $T_N$ , which is seen for both Mn 3s and Mn 3p.

(vii) The observation of a large (0.4 eV) narrowing of the 3d valence bands in going above  $T_N$ , with no effect being seen in going through  $T_{\text{SR}}$ .

(viii) A qualitative agreement between experiment and a single-scattering theory of such core-level SPPD effects<sup>2</sup> as to the magnitudes and in some cases also the signs of the steps observed, particularly for domain I antiferromagnetic ordering.

The above observations thus provide strong evidence for a short-range magnetic phase transition at  $T_{\text{SR}}$  that has not previously been observed. Although we cannot say for certain from this rather surface-sensitive data whether this transition is a phenomenon unique to the surface or extends further into the bulk, our results indicate that it extends at least a few layers in from the sur-

face.

Although there is as yet no quantitative theory of such a high-temperature short-range magnetic transition, we suggest that it qualitatively represents the final breakup of small domains of antiferromagnetic order that may extend over only the first few spheres of magnetic neighbors around a given  $\text{Mn}^{2+}$  emitter. Below  $T_{\text{SR}}$ , these domains may have fluctuation times longer than the very-short-time scale of  $10^{-16}$ – $10^{-17}$  sec that is involved in the photoemission process. It is also intriguing that, for both materials studied to date, the  $T_{\text{SR}}$  value is quite close to the relevant Curie-Weiss constant  $\Theta$ :  $T_{\text{SR}}/\Theta \approx 0.99$  for  $\text{KMnF}_3$  and  $T_{\text{SR}}/\Theta \approx 0.92$  for MnO. Since  $\Theta$  in mean-field theory can be shown to represent a sum over near-neighbor interaction energies,<sup>24</sup> it may be reasonable that these small domains are finally destroyed at a comparable temperature. However, there is as yet no quantitative theoretical connection of  $\Theta$  with  $T_{\text{SR}}$ .

It is thus clear that further experimental and theoretical work is necessary to better establish the systematics of such SPPD effects and to fully understand their origin. However, even in the absence of such a detailed understanding, the results obtained to date indicate that SPPD provides a rather unique measure of the temperature at which short-range magnetic order with very-short-time scales is ultimately lost. There is also evidence that SPPD is sensitive to the breakdown of long-range order.

#### ACKNOWLEDGMENTS

This work has been supported by the Office of Naval Research (Contracts No. N00014-87-K-0512 and No. N00014-90-J-1457), U.S. Department of Defense and the National Science Foundation (Grant No. CHE-83-20200). Two of us (B.D.H. and D.F.J.) gratefully acknowledge support by IBM and another (C.S.F.) support by the University of Hawaii and by the University of Paris. We are also grateful to Dr. V. Jaccarino for supplying us with the MnO crystal used.

\*Present address: IBM Research Division, Almaden Research Center, 650 Harry Road, San Jose, CA 95120-6099.

†Present address: Department of Physics, University of Fribourg, CH-1700 Fribourg, Switzerland.

‡Present address: Solar Energy Research Institute, 1617 Cole Boulevard, Golden, CO 80401.

§Present address: Department of Physics, New York University, 4 Washington Place, New York, NY 10003.

<sup>1</sup>(a) C. S. Fadley (unpublished); (b) G. M. Rothberg, *J. Magn. Mater.* **15-18**, 223 (1980).

<sup>2</sup>(a) B. Sinkovic and C. S. Fadley, *Phys. Rev. B* **31**, 4665 (1985); (b) B. Sinkovic, D. J. Friedman, and C. S. Fadley, (unpublished); (c) D. J. Friedman, B. Sinkovic, and C. S. Fadley, *Phys. Scr.* (to be published); (d) D. J. Friedman, A. P. Kaduwela, D. R. Boucher, and C. S. Fadley (unpublished).

<sup>3</sup>B. Sinkovic, B. Hermsmeier, and C. S. Fadley, *Phys. Rev. Lett.* **55**, 1227 (1985).

<sup>4</sup>B. Hermsmeier, B. Sinkovic, J. Osterwalder, and C. S. Fadley, *J. Vac. Sci. Technol. A* **5**, 1082 (1987).

<sup>5</sup>M. T. Johnson, H. I. Starnberg, and H. P. Hughes, *J. Phys. C* **20**, 4385 (1987).

<sup>6</sup>R. Feder, *Polarized Electrons in Surface Physics* (World Scientific, Singapore, 1985).

<sup>7</sup>J. Kischner, *Polarized Electrons at Surfaces* (Springer-Verlag, Berlin, 1985).

<sup>8</sup>D. T. Pierce and R. J. Celotta, *J. Vac. Sci. Technol. A* **1**, 1119 (1983); D. T. Pierce and R. J. Celotta, in *Advances in Electronics and Electron Physics*, edited by C. Marton (Academic, New York, 1981), Vol. 56.

<sup>9</sup>B. Babic, N. B. Neskovic, and J. Konstantinovic, *Fiz.* **8**, 257 (1976); C. G. Shull, W. A. Strause, and E. O. Wollan, *Phys. Rev.* **83**, 333 (1951).

<sup>10</sup>C. Rau, *J. Magn. Mater.* **30**, 141 (1982).

<sup>11</sup>C. S. Fadley, D. A. Shirley, A. J. Freeman, P. S. Bagus, and J. V. Mallow, *Phys. Rev. Lett.* **23**, 1397 (1969); C. S. Fadley and D. A. Shirley, *Phys. Rev. A* **2**, 1109 (1970).

<sup>12</sup>P. S. Bagus, A. J. Freeman, and F. Sasaki, *Phys. Rev. Lett.* **30**, 850 (1973).

- <sup>13</sup>S. P. Kowalczyk, L. Ley, R. A. Pollak, F. R. McFeely, and D. A. Shirley, *Phys. Rev. B* **7**, 4009 (1973); S. P. Kowalczyk, Ph.D. thesis, University of California at Berkeley Report No. LBL-4319, 1976.
- <sup>14</sup>J. C. Carver, G. K. Schweitzer, and T. A. Carlson, *Chem. Phys.* **57**, 973 (1972); R. L. Cohen, G. K. Wertheim, A. Rosencwaig, and H. J. Guggenheim, *Phys. Rev. B* **5**, 1037 (1972); F. R. McFeely, S. P. Kowalczyk, L. Ley, and D. A. Shirley, *Phys. Lett.* **49A**, 301 (1974).
- <sup>15</sup>C. S. Fadley, in *Electron Spectroscopy: Theory, Techniques, and Applications*, edited by C. R. Brundle and A. D. Baker (Academic, London, 1978), Vol. 2, Chap. 1.
- <sup>16</sup>(a) B. Hermsmeier, C. S. Fadley, M. O. Krause, J. Jimenez-Mier, P. Gerard, and S. T. Manson, *Phys. Rev. Lett.* **61**, 2592 (1988); V. Kinsinger, I. Sander, P. Steiner, R. Zimmerman, and S. Huefner, *Solid State Commun.* **73**, 527 (1990).
- <sup>17</sup>R. K. Nesbet, *Phys. Rev. B* **32**, 390 (1985).
- <sup>18</sup>(a) C. S. Fadley, *Prog. Surf. Sci.* **16**, 275 (1984); (b) C. S. Fadley, *Phys. Scr.* **T17**, 39 (1987); (c) M. Sagurton, E. L. Bullock, and C. S. Fadley, *Surf. Sci.* **182**, 287 (1987); (d) E. L. Bullock and C. S. Fadley, *Phys. Rev. B* **31**, 1212 (1985); C. S. Fadley, in *Synchrotron Radiation Research: Advances in Surface and Interface Science*, edited by R. Z. Bachrach (Plenum, New York, in press).
- <sup>19</sup>R. Feder (private communication).
- <sup>20</sup>S. Hara, *J. Phys. Soc. Jpn.* **22**, 710 (1967).
- <sup>21</sup>W. Kohn and L. J. Sham, *Phys. Rev.* **140**, A1133 (1965).
- <sup>22</sup>G. A. Costa, G. Granozzi, B. D. Hermsmeier, and C. S. Fadley (unpublished).
- <sup>23</sup>L. J. de Jonge and A. R. Miedema, in *Advances in Physics*, edited by B. R. Coles and D. H. Martin (Taylor and Francis, London, 1974), Vol. 23, No. 1.
- <sup>24</sup>J. E. Smart, *Effective Field Theories of Magnetism* (Saunders, New York, 1966), Chap. 4.
- <sup>25</sup>J. M. Sanchez and J. L. Moran-Lopez, *Phys. Rev. Lett.* **58**, 1120 (1987) and private communication; and discussion of these results by C. S. Fadley, in *Magnetic Properties of Low-Dimensional Systems II*, edited by L. M. Falicov, F. Mejia-Lira, and J. L. Moran-Lopez (Springer-Verlag, Berlin, 1990), p. 36.
- <sup>26</sup>C. Noguera and D. Nigel (private communication).
- <sup>27</sup>B. Hermsmeier, J. Osterwalder, D. J. Friedman, and C. S. Fadley, *Phys. Rev. Lett.* **62**, 478 (1989).
- <sup>28</sup>E. Schleiter-Steinkopf, *Gmelin Handbook of Inorganic Chemistry: Manganese* (Verlag Chemie, Weinheim, 1973), Vol. C1.
- <sup>29</sup>B. Morosin, *Phys. Rev. B* **1**, 236 (1970).
- <sup>30</sup>Y. S. Touloukian and E. H. Buyco, *Thermophysical Properties of Matter: Specific Heat* (Plenum, New York, 1970), Vol. 5.
- <sup>31</sup>J. Osterwalder, M. Sagurton, P. J. Orders, C. S. Fadley, B. Hermsmeier, and D. J. Friedman, *J. Electron. Spectros. Relat. Phenom.* **48**, 55 (1989).
- <sup>32</sup>The Mo-coated Cu anode was developed by H. R. Scherrer, Physics Department, ETH, Zürich, Switzerland.
- <sup>33</sup>L. Z. Shao and V. Young, *J. Electron. Spectrosc. Relat. Phenom.* **34**, 1 (1984).
- <sup>34</sup>H. K. Hu and J. W. Rabalais, *Surf. Sci.* **107**, 376 (1981).
- <sup>35</sup>M. Oky, K. Hirokawa, and S. Ikeda, *J. Electron. Spectrosc. Relat. Phenom.* **7**, 465 (1975).
- <sup>36</sup>A. J. Bosman and H. J. van Daal, *Advances in Physics* (Taylor and Francis, London, 1970), Vol. 19.
- <sup>37</sup>R. Saiki, A. Kaduwela, J. Osterwalder, M. Sagurton, C. S. Fadley, and C. R. Brundle, *J. Vac. Sci. Technol. A* **5**, 932 (1987); R. Saiki, A. P. Kaduwela, J. Osterwalder, C. S. Fadley, and C. R. Brundle, *Phys. Rev. B* **40**, 1586 (1989); R. Saiki *et al.* (unpublished).
- <sup>38</sup>J. J. Barton and D. A. Shirley, *Phys. Rev. B* **32**, 1892 (1985); **32**, 1906 (1985); W. Egelhoff, *J. Vac. Sci. Technol. A* **2**, 350 (1984); *Phys. Rev. B* **30**, 1052 (1984).
- <sup>39</sup>J. Osterwalder, E. A. Stewart, D. Cyr, C. S. Fadley, J. Mustre de Leon, and J. J. Rehr, *Phys. Rev. B* **35**, 9859 (1987).
- <sup>40</sup>T. Yamaguchi, S. Shibuya, and S. Sugano, *J. Phys. C* **15**, 2625 (1982).
- <sup>41</sup>(a) C. Carbone and E. Kisker, *Solid State Commun.* **65**, 1107 (1988); (b) B. Sinkovic, P. D. Johnson, N. B. Brookes, A. Clarke, and N. V. Smith (unpublished).
- <sup>42</sup>K. Binder, *Monte Carlo Methods in Statistical Physics* (Springer-Verlag, New York, 1979).
- <sup>43</sup>Y. A. Izyumov and R. P. Ozerov, *Magnetic Neutron Diffraction* (Plenum, New York, 1970).
- <sup>44</sup>M. S. Kushwaha, *Physica B+C* (Amsterdam) **112B**, 232 (1982).
- <sup>45</sup>E. J. Ojala and K. Terakura, *Phys. Rev. B* **33**, 2733 (1986).
- <sup>46</sup>A. Bakhshai, L. M. Holaday, G. D. Eknayan, and N. E. Brener, *Phys. Rev. B* **29**, 6932 (1984).
- <sup>47</sup>M. P. Seah and D. P. Dench, *Surf. Int. Anal.* **1**, 2 (1979).
- <sup>48</sup>I. Suzuki, S. Okajima, and K. Seya, *J. Phys. Earth* **27**, 63 (1979); D. Basu and J. K. D. Verma, *J. Pure Appl. Phys.* **18**, 204 (1980); K. G. Subhadra and D. B. Sirdeshnukh, *ibid.* **16**, 693 (1978).
- <sup>49</sup>S. Ohnishi, A. J. Freeman, and M. Weinert, *Phys. Rev. B* **28**, 6741 (1983).